

Overcharging and charge reversal in the electrical double layer near the point of zero charge

G. Iván Guerrero-García,^{1,2} Enrique González-Tovar,¹ Martín Chávez-Páez,¹ and Marcelo Lozada-Cassou²

¹*Instituto de Física, Universidad Autónoma de San Luis Potosí,
Álvaro Obregón 64, 78000 San Luis Potosí, S.L.P., México*
²*Programa de Ingeniería Molecular, Instituto Mexicano del Petróleo,
Eje Central Lázaro Cárdenas Norte 152, 07730 México, D.F., México*

(Dated: October 9, 2018)

The ionic adsorption around a weakly charged spherical colloid, immersed in size-asymmetric 1:1 and 2:2 salts, is studied. We use the primitive model of an electrolyte to perform Monte Carlo simulations as well as theoretical calculations by means of the hypernetted chain/mean spherical approximation (HNC/MSA) and the unequal-radius modified Gouy-Chapman (URMGC) integral equations. Structural quantities such as the radial distribution functions, the integrated charge, and the mean electrostatic potential are reported. Our Monte Carlo “experiments” evidence that near the point of zero charge the smallest ionic species is preferentially adsorbed onto the macroparticle, independently of the sign of the charge carried by this tiniest electrolytic component, giving rise to the appearance of the phenomena of charge reversal and overcharging. Accordingly, charge reversal is observed when the macroion is slightly charged and the coions are larger than the counterions. In the opposite situation, i.e. if the counterions are larger than the coions, overcharging occurs (a feature originally predicted via integral equations in J. Phys. Chem. B **108**, 7286 (2004), for the planar electrical double layer). In other words, *in this paper we present the first simulational data on overcharging*, showing that this novel effect surges, close to the point of zero charge, as a consequence of the ionic size asymmetry. We also find that the HNC/MSA theory captures well the charge reversal (CR) and overcharging (OC) phenomena exhibited by the computer “experiments”, especially as the macroion’s charge increases. On the contrary, even if URMGC also displays CR and OC, its predictions do not compare favorably with the Monte Carlo results. Further, it is seen that the inclusion of hard-core correlations in Monte Carlo and HNC/MSA leads to spatial regions near the macroion’s surface in which the integrated charge and/or the mean electrostatic potential can decrease when the colloidal charge is augmented and vice versa. These observations aware about the interpretation of electrophoretic mobility measurements using the standard Poisson-Boltzmann approximation beyond its validity region.

PACS numbers: 61.20.-p, 61.20.Gy, 61.20.Ja, 61.20.Qg.

I. INTRODUCTION

It is widely known in physical-chemistry that a surface in contact with an electrolyte solution usually becomes charged and, thus, that the ions around the interface acquire a diffuse structure commonly denoted as the electrical double layer (EDL). One of the most successful early theories used to describe these systems in the dilute and/or weak electrostatic regimes is the classic Poisson-Boltzmann (PB) treatment, which is based on a point-ions representation of an electrolyte [1, 2, 3]. Under this approach, it is an accepted fact that the counterions of a binary electrolyte are mostly adsorbed to the electrode when its surface charge density is increased; the coions, on the other hand, are pushed away from the region close to the charged surface [2, 4]. As a result, in the PB picture, the main role of the EDL is to neutralize *monotonically* the surface charge as a function of the distance to the macroparticle, leading to a screened interaction between charged colloids in solution [5]. However, starting from the middle of the past century, an appreciable number of experimental instances has been detected in which the effective charge of a colloid seems to reverse its sign (recent electrophoresis papers can be

consulted in Refs. [6, 7, 8]). This singularity, due to an excess in the counterion’s compensation of the bare surface charge, is known as charge reversal (CR), and the too simplified PB formalism can not describe it since its occurrence involves strong ion-size correlations. It must be noted that, despite a lot of experimental research, it was only until recent times that direct measurements of CR were performed by Besteman et al. [9, 10, 11], who employed atomic force microscopy techniques and a new electrophoresis capillarity apparatus to achieve laboratory conditions that were very difficult, or even impossible, to reach in traditional static and electrokinetic experiments.

Through the years, the experimental advances have prompted the development of theoretical explanations for CR. In this way, the strong correlated liquid formalism [12] was conceived as an effort to comprehend and predict this kind of behavior. For macroparticles dissolved in trivalent electrolytes this scheme yields information consistent with observational data, but breaks down when applied to divalent solutions [11]. Alternatively, the theory of integral equations for liquids has proved to be a robust and reliable approach in this area of research [1, 13, 14, 15, 16, 17, 18, 19, 20]. For in-

stance, it has been the main route to demonstrate that the ionic excluded volume constitutes, by itself, a physical mechanism with the ability to induce charge reversal [21], although this does not mean, naturally, that the CR observed experimentally under very diverse conditions is due purely to such steric effects (an interesting discussion about the physical and/or chemical origins of CR is available in [22]).

Another fascinating phenomenon that has been theoretically predicted to occur in the EDL is overcharging (OC). OC appears when the coions are adsorbed to the electrified interface, despite the coulombic repulsion, *increasing* the native surface charge. This anomaly was first observed and defined for a mixture of macroions and a size-symmetric electrolyte in contact with a charged wall [23]. Notably, in such article the goal was to establish that the overcharging was prompted by the macroions, whereas here we will show that OC can be present even in a simpler system (without a wall) if ionic size asymmetry comes into play. In this context, it is worth to recall that the most basic way to incorporate *consistently* ionic size contributions into the EDL is by using the so-called primitive model (PM) of an electrolyte, wherein the ions are taken as hard spheres with point charges embedded at their centers. A large amount of work has been reported for the EDL using the PM in the special case of equal-sized ions (i.e. the restricted primitive model (RPM)), which implies a considerable simplification at the level of the model and calculations [13, 14, 15, 16, 17, 18, 21, 24, 25, 26, 27, 28, 29, 30, 31, 32, 33]. Notwithstanding, it is more realistic to expect EDL systems with different ionic sizes in their electrolytic species (due, for instance, to a distinct degree of hydration of the ions) and, thus, the PM should be preferred for a more faithful representation of the EDL.

Along these lines, the issue of the practical relevance of ionic size asymmetry in the physical-chemistry of surfaces has been recently revived in an experimental paper on the electrokinetics of uncharged colloids by Dukhin et al. [34]. In such investigation, the authors revisited the idea that "...a double layer might in fact exist, even when there is no electric surface charge at all (on the colloid), solely because of the difference in cation and anion concentrations within the interfacial water layer..." and provided a measurement technique and experimental data supporting the existence of the so-called zero surface charge double layer, a concept introduced in a theoretical model by Dukhin himself and coworkers more than two decades ago [35, 36, 37]. The relevant fact to our discussion is that, as proposed by Dukhin and other authors [38, 39, 40, 41, 42, 43], such a difference in cation and anion concentrations, and the concomitant charge separation in the proximity of an uncharged colloid, can be attributed to the difference in the distances of closest approach of counterions and coions to the surface (as an alternative, or in addition, to the "chemical" phenomenon of specific adsorption). Thence, the work by Dukhin et al. emphasizes the importance of the ionic size asymme-

try effect in relevant phenomena occurring in real EDL systems, like the binding of simple inorganic electrolyte ions on colloidal substrates, and electrokinetics.

It is interesting that in the literature there are relatively few publications considering ionic size asymmetry (see, for example, [5, 44, 45, 46, 47, 48, 49, 50, 51, 52, 53, 54]), most of them dedicated to the planar geometry and only two reports for the spherical case [5, 54]. In our opinion, this apparent lack of interest in size-asymmetric electrolytes might arise from the long-standing belief in the dominance of counterions in the EDL; a fact foreseen and corroborated in a couple of pioneering papers on the modified Gouy-Chapman (MGC) theory for planar interfaces [44, 45]. To be more explicit, the precise meaning of the dominance of counterions is that "...at large potentials or charge densities, the coions are excluded from the vicinity of the electrode. Consequently, the counterions dominate and the double layer properties approach those of a symmetric electrolyte whose charge and diameter are equal to those of the counterions..." [45]. Noticeably, and even if this behavior was originally enunciated and verified *exclusively at the MGC level*, during the past years most of the modern studies of the EDL, that use theoretical approaches which surpass the punctualions PB treatment, have subscribed (or assumed without a rigorous proof) such counterion predominance in the primitive model [1, 29, 47, 48, 51, 55, 56, 57], a situation that has resulted in the mentioned scant attention to size-asymmetric EDLs. In contrast, very recently, some of the present authors have published an integral equation and simulational analysis of the size-asymmetric spherical EDL [5] where it has been evidenced that, for highly charged surfaces, counterions do not always dominate, i.e. that coions really matter in the double layer. At this point, it should be also noted that the establishment of the counterion dominance by Valleau, Bhuiyan and coworkers [44, 45] was not really based on the *plain* Poisson-Boltzmann equation, or equivalently on a model of a genuine punctual electrolyte, since for these authors the ion-ion potential corresponds to that between point charges whereas for the ion-wall interaction a closest approach distance (hard-core or Stern correction) is added. In fact, the unequal radius modified Gouy-Chapman (URMGC) approach of Refs. [44, 45] represents not only the inclusion, at the lowest order, of excluded volume contributions into the Gouy-Chapman theory (via the Stern modification), but also the first attempt to take into account the ionic size asymmetry through the use of different distances of closest approach for counterions and coions. From all the above discussed, the new integral equations results for a colloid in contact with a size-asymmetric PM electrolyte [5, 54] (in which hard-core contributions are consistently embodied in both the ion-surface and ion-ion interactions) imply that an incomplete consideration of excluded volume and size asymmetry contributions, like that of the URMGC theory, can lead to an inaccurate description of the double layer at high surface charges.

On the other hand, apart from the dominance of counterions at large electric fields, URMGC has predicted other notable phenomena in the EDL, this time for low charged surfaces, such as the appearance of a potential of zero charge, oscillations in the ionic density and mean electrostatic potential functions, and indeed charge reversal and overcharging [58, 59]. Lately, several theoretical and simulational investigations [51, 53, 60] have pondered the planar EDL for a PM electrolyte in the low-charge regime and have corroborated the existence of the potential of zero charge and the non-monotonic behavior of the ionic radial distribution functions (RDFs) and potential profiles, previously seen in the “semi-punctual” URMGC. Nevertheless, in the same reports it was also found that only those theoretical formalisms (e.g. the MPB5 and density functional theories) that fully include the hard-core and ionic size asymmetry effects succeeded in describing quantitatively the EDL near the point of zero charge [53, 60], contrasting with URMGC that showed solely a limited success for 1:1 salts [51]. In addition, and with respect to CR and OC, in a 2006 paper [58] Yu et al. noticed, for the first time, the appearance of these “anomalies” in an URMGC treatment of an electrolyte in a charged slit; a certainly intriguing fact given that, in the past, CR and OC had been observed only in theoretical analysis of primitive model EDLs [21, 23]. Therefore, at present, an exhaustive simulation study that confirms and characterizes the phenomena of charge reversal and overcharging in *slightly* charged PM EDLs, as well as an application of reliable theories in order to explain these striking features, is still lacking in the literature. Precisely, the main objectives of this communication are, in the first place, to supply fresh and comprehensive Monte Carlo (MC) data about the potential of zero charge, charge reversal, overcharging and the behavior of diverse structural properties of a low charged primitive model EDL in spherical geometry and, secondly, to present the comparison of such simulational information with the corresponding theoretical results of the HNC/MSA and URMGC integral equations, trying to assess the consequences of a consistent treatment of the excluded volume and ionic size asymmetry contributions in the spherical electrical double layer.

To investigate the static properties of the size-asymmetric spherical EDL in the weakly charged regime, with special focus on the CR and OC phenomena, we have produced simulation and HNC/MSA integral equation results for the radial distribution functions (RDFs) of 1:1 and 2:2 primitive model electrolytes bathing a spherical colloid under diverse conditions. From the RDFs we extract the mean electrostatic potential and the charge profiles to identify the presence of charge reversal and overcharging and to examine their dependence on the ionic size asymmetry and other system parameters. All this structural information is contrasted with that corresponding to the semi-punctual URMGC theory. As it will be illustrated below, most of the computer “experiments” data are better paralleled by HNC/MSA

than by URMGC. Additionally, we would like to note that, to the best of our knowledge, this work reports the first confirmation, via simulations, of charge reversal and overcharging in the EDL near the point of zero charge. This paper is organized as follows. In Section II we present the model system and the theoretical approaches. Section III contains the details of the numerical solution of the integral equations and of the Monte Carlo simulations. Section IV is devoted to the results and their discussion, and we close with a summary of relevant findings and conclusions in Section V.

II. MODEL SYSTEM AND THEORY

Our basic representation of the spherical electrical double layer (SEDL) is constituted by a rigid, charged spherical colloid of diameter D_0 and uniform surface charge density σ_0 , surrounded by a continuum solvent of dielectric constant ϵ . The macroion is in contact with two ionic species, which in the primitive model are treated as hard spheres of diameters D_i ($i = 1, 2$) with embedded point charges, q_i , at their centers. Note that $q_1 q_2 < 0$. The interaction potential between the particles in this model (i.e. macroion and electrolytic ions) is then given by

$$U_{ij}(r) = \begin{cases} \infty, & \text{for } r < D_{ij}, \\ q_i q_j / (\epsilon r), & \text{for } r \geq D_{ij}, \end{cases} \quad (1)$$

where the subscripts i and j run from 0 to 2, r is the center-to-center distance between two particles of types i and j , $D_{ij} = (D_i + D_j)/2$, $q_i = z_i e$ is the charge of the species i with valence z_i , e is the protonic charge, and, for the spherical colloid, $q_0 = z_0 e = 4\pi(D_0/2)^2 \sigma_0$. The system as a whole is electroneutral, i.e. $\sum_{j=1}^2 z_j \rho_j = 0$, where ρ_j is the bulk number density of the electrolytic species j .

The Ornstein-Zernike equation for a multicomponent mixture of S species is [61]

$$h_{ij}(r) = c_{ij}(r) + \sum_{k=0}^{S-1} \rho_k \int h_{ik}(t) c_{kj}(|\vec{r} - \vec{t}|) dV, \quad (2)$$

such as ρ_i is the bulk number density of each one of the species in the system, $r = |\vec{r}|$ and $h_{ij}(r)$ are, respectively, the distance and the total correlation function between two particles of types i and j , $g_{ij}(r) = h_{ij}(r) + 1$ is the radial distribution function, $c_{ij}(r)$ is the direct correlation function, and $t = |\vec{t}|$ being the distance between two particles of types i and k . This group of equations requires a second relation (or closure) between the total and direct correlation functions. For charged systems, the hypernetted chain (HNC) and the mean spherical approximation (MSA) closures are widely used [61, 62]. The HNC and MSA relations, for $r \geq D_{lm}$, are given as:

$$c_{lm}(r) = -\beta U_{lm}(r) + h_{lm}(r) - \ln[h_{lm}(r) + 1], \quad (3)$$

for HNC, and

$$c_{lm}(r) = -\beta U_{lm}(r), \quad (4)$$

for MSA, where $\beta = 1/(k_B T)$ is the inverse of the thermal energy. These expressions are complemented by the exact condition $h_{lm}(r) = -1$, for $r < D_{lm}$.

Let us consider $S = 3$ and that the species 0 corresponds to macroions (thereinafter denoted equivalently by M) at infinite dilution, whereas the indices 1 and 2 are associated to a binary electrolyte. Then Eq. (2) for the components $M(\equiv 0)$ and j can be written as:

$$h_{Mj}(r) = c_{Mj}(r) + \sum_{k=1}^2 \rho_k \int h_{Mk}(t) c_{kj}(|\vec{r} - \vec{t}|) dV, \quad (5)$$

$j = 1, 2.$

Note that Eqs. (5) are a complete set of integral equations for the SEDL. When Eq. (3) is employed in Eqs. (5) solely for $c_{Mj}(r)$, and the $c_{kj}(|\vec{r} - \vec{t}|)$ are approximated by the MSA analytical expressions for a bulk electrolyte [63, 64, 65], the HNC/MSA integral equations are obtained. A detailed account of this HNC/MSA formalism can be consulted elsewhere [5] and will not be repeated here. Our election of the HNC/MSA theory to perform the present study is based on the fact that, for many years, it has been used successfully to investigate the RPM electrical double layer in many geometries (e.g. planar, cylindrical, and spherical) [5, 14, 16, 17, 66, 67].

The integral version of the URMGC theory in *spherical geometry* is easily deduced from the HNC/MSA formulation if $c_{kj}(|\vec{r} - \vec{t}|) = -\beta q_k q_j / (\epsilon |\vec{r} - \vec{t}|)$ is inserted in Eqs. (5), instead of the inter-ionic MSA direct correlation functions. It must be stressed that, in the original papers [44, 45], as well as in all the posterior treatments [51], URMGC has been solved, in differential form, strictly for planar interfaces, which means that the present study extends the classic URMGC planar theory to the spherical instance, continuing along the lines of our previous URMGC (and HNC/MSA) account of the SEDL [5].

Once the $g_{Mj}(r)$ are available, either from a theory (e.g. HNC/MSA or URMGC) or from simulation, it is then possible to calculate various relevant functions, namely the local electrolyte charge density (LECD),

$$\rho^*(r) = \sum_{j=1}^2 z_j \rho_j g_{Mj}(r) 4\pi r^2, \quad (6)$$

the total integrated charge (IC),

$$P(r) = z_M + \int_0^r \rho^*(t) dt, \quad (7)$$

and the mean electrostatic potential (MEP),

$$\psi(r) = \frac{e}{\epsilon} \int_r^\infty \frac{P(t)}{t^2} dt. \quad (8)$$

These quantities are fundamental in our analysis of the properties of the SEDL. The LECD is a linear density that gives us information about the electrolytic charge (in units of e) inside a spherical shell of thickness dr located at a distance r from the center of the macroion. Besides, the integral over all the space of $-\rho^*(r)$ results in the valence of the macroion, z_M , as required by the electroneutrality condition. On the other hand, the IC is a measure of the net charge (in units of e) enclosed in a sphere of radius r centered in the macroion. It equals z_M for $D_0/2 \leq r \leq (D_0 + D_1)/2$, if $D_1 < D_2$, and goes to zero as $r \rightarrow \infty$, again due to the electroneutrality restriction. The IC also allows to compute the amount of charge adsorbed onto the macroparticle, i.e. the accumulated charge within the Helmholtz planes (see below for the definition of the Helmholtz planes), and, moreover, it detects charge reversal when $P(r)z_M < 0$, and overcharging if $P(r)z_M > 0$ and $|P(r)| > |z_M|$. In addition, the MEP around the macroion is a central magnitude in colloid science because it determines, for instance, the regimes of stability/flocculation or the migration of macroparticles in a colloidal suspension [68]. As a matter of fact, the MEP at certain distance near the macroion's surface is usually identified with the well-known electrokinetic potential at the slipping plane (or zeta potential, ζ) [4]. The ζ potential is experimentally measurable in systems that display electrokinetic effects such as electrophoresis, electro-osmosis and streaming currents, and it has an ample use in the physico-chemical characterization, separation and/or fabrication of colloidal materials [2, 69].

In particular, we will be interested in the IC and the MEP in the neighborhood of the Stern layer. More specifically, the Stern layer is the free-of-ions space next to a macroion that ends at the Helmholtz plane. The Helmholtz plane (or, more properly, the Helmholtz surface) is the geometrical place associated to the colloid-ion closest approach distance [4, 68]. In size-symmetric electrolytes only one Helmholtz plane can be identified. In our model, however, the size asymmetry between the ions allows us to define an inner Helmholtz "plane" (IHP) and an outer Helmholtz "plane" (OHP) (note the conventional usage of the word "plane"). The IHP is specified by the closest approach distance of the smallest ionic component to the colloidal surface (i.e., by $(D_0 + D_1)/2$, if $D_1 < D_2$), whereas the OHP is determined by the corresponding distance of closest approach for the largest species (i.e., by $(D_0 + D_2)/2$, if $D_1 < D_2$). Therefore, for the primitive model EDL, if $D_1 < D_2$, the Stern layer is the region where $D_0/2 \leq r < (D_0 + D_1)/2$, and the Helmholtz zone corresponds to $(D_0 + D_1)/2 \leq r \leq (D_0 + D_2)/2$. Obviously, for size-symmetric salts the IHP and the OHP coincide and the standard notions of the Helmholtz plane and Stern layer are recovered. In the

general PM case, and provided that $D_1 < D_2$, when the MEP is evaluated at $r = (D_0 + D_1)/2$, Eq. (8) gives the MEP at the IHP, which we denote as ψ_{IHP} . On the other hand, if Eq. (8) is calculated at $r = (D_0 + D_2)/2$, the MEP at the OHP, ψ_{OHP} , is obtained.

III. NUMERICAL DETAILS

A size-asymmetric 1:1 or 2:2 electrolyte with a ratio between ionic diameters $D_-/D_+ = 2$, bathing a charged macroparticle of diameter $D_M = D_0 = 20 \text{ \AA}$ and valence z_M , was considered in all the calculations reported. Specifically, the diameters of the positive and negative species were $D_+ = 4.25 \text{ \AA}$ and $D_- = 8.5 \text{ \AA}$, respectively. In other words, for definitiveness, the cations have been chosen as the smallest species of the binary electrolyte, i.e., $D_+ = D_1$ and $D_- = D_2$, with $D_1 < D_2$. Note also that the sign of z_M defines which one of the ionic species is the coion or counterion.

To establish the primitive and semi-punctual models employed in our simulational and theoretical approaches, let us introduce the macroion-ion contact distances, d_{M+} and d_{M-} , given by

$$d_{Ml} = \begin{cases} (D_M + D_+)/2, & \text{for } l = +, \text{ in simulation,} \\ & \text{HNC/MSA and URMGC,} \\ (D_M + D_-)/2, & \text{for } l = -, \text{ in simulation,} \\ & \text{HNC/MSA and URMGC.} \end{cases} \quad (9)$$

It must be remembered that here the macroions, cations and anions correspond to the indices 0, 1 and 2, respectively.

Complementarily, the ion-ion contact distances, d_{++} , d_{--} , and $d_{+-}(=d_{-+})$, are

$$d_{ij} = \begin{cases} D_+, & \text{for } i = j = +, \text{ in simulation} \\ & \text{and HNC/MSA,} \\ D_-, & \text{for } i = j = -, \text{ in simulation} \\ & \text{and HNC/MSA,} \\ (D_+ + D_-)/2, & \text{for } i = + \text{ and } j = -, \text{ in simulation} \\ & \text{and HNC/MSA,} \\ 0, & \text{for any } i \text{ and } j, \text{ in URMGC.} \end{cases} \quad (10)$$

The dielectric constant and temperature considered in all the cases were $\epsilon = 78.5$ and $T = 298 \text{ K}$.

The URMGC and HNC/MSA theories were numerically solved by means of a Picard iteration scheme, which, in the past, has been thrivingly employed in a number of studies of the EDL in various geometries via integral equations and density functional theories [5, 29, 33].

Simulations were performed in a cubic box with the usual periodic boundary conditions in the canonical ensemble. The ionic species satisfied the electroneutrality condition: $z_M + N_+z_+ + N_-z_- + N_cz_c = 0$, where z_M is the valence of the macroion, N_+ , z_+ and N_- , z_- are

the number of ions and the valence of the positive and negative electrolytic species, respectively, and N_c and z_c are the number and the valence of the counterions that balance the colloidal charge. In order to accomplish consistent comparisons with the theory, the absolute value of the valence of such counterions was $|z_c| = 1$ for the 1:1 electrolyte and $|z_c| = 2$ for the 2:2 salt. The macroion was fixed in the center of a simulation box of length L and, in order to avoid border effects, the extension of the cell was enlarged until the integrated charge showed clearly a plateau of zero charge far from the macroion. The runs were done for ≈ 2000 particles for the monovalent salt and ≈ 1000 ions for the divalent electrolyte. The long-range interactions were taken into account by using the Ewald sum technique with conducting boundary conditions [70, 71]. The associated damping parameter was $\alpha = 5/L$ and the \vec{k} -vectors employed to compute the reciprocal space contribution satisfied the condition $|\vec{k}| \leq 5$. Monte Carlo runs of charged systems were performed with 5×10^4 equilibration MC cycles and from 6×10^5 to 1.8×10^6 MC cycles were practised for the production stage. The radial distribution functions were calculated using standard bin procedures [70, 71], whereas the integrated charge and the electrostatic potential were obtained by using Eqs. (7) and (8), respectively.

IV. RESULTS AND DISCUSSION

In what follows, our results are discussed chiefly in terms of the Monte Carlo (MC) simulations data. Appropriate comparisons with the HNC/MSA and URMGC formalisms are presented such that the accuracy of the theoretical predictions can be assessed.

A. Monovalent size-asymmetric electrolytes

The structure of the EDL is the result of an entropic and energetic competition. In the proximities of the point of zero charge the entropy is expected to be important, whereas for highly charged macroparticles the EDL is expected to exhibit strong coulombic correlations. Thus, in order to understand the behavior of the ionic atmosphere next to a barely charged colloid in contact with a size-asymmetric electrolyte, we will first present a comparison between the surrounding distribution of a univalent salt and that of a mixture of hard spheres having the same radii and concentration. This will illustrate how the structure of charged systems deviate from the neutral situation.

Let us consider initially the ionic distribution around an uncharged macrosphere ($z_M = 0$). Fig. 1 (main panel) displays the radial distribution functions (RDFs) of two systems; in one case the ionic species represent a 1:1, 1 M salt, and in the other the ions are uncharged, forming a pure hard-sphere assembly. We note here that, in the former system, the EDL is the result of both

the entropic and energetic contributions; in contrast, the structure of the latter instance is only driven by entropy because all the interactions are of the excluded volume type. Nevertheless, since we are working in the zero colloidal charge regime, we expect that in the first case the excluded volume interactions must play a determinant role in the resulting properties of the double layer. The direct comparison of the simulational and theoretical RDFs of the charged and uncharged spheres around the neutral macroion is presented in the main panel of Fig. 1. An inspection of the Monte Carlo data shows that the structure of the two mixtures (of ions and of the hard spheres) is rather similar for $r'/D_+ > 2.5$ (where r' is the distance measured from the colloidal surface), indicating the existence of weak charge correlations at these distances. Differences, however, are noticeable at smaller distances, particularly for the tiniest species. We observe that the addition of charge to the ionic species slightly increases the concentration of the larger species and decreases the concentration of the smaller species, especially at the contact distances. As it is shown later, this dewetting of the surface augments with the valence of the ions. Such comportment of the RDFs could lead eventually to significant changes in the thermophysical properties of the charged systems since, for instance, the pressure depends directly on the contact values of the pair correlation functions [62]. We must point out that these are rather concentrated systems, with an ionic volume fraction of $\phi \approx 0.217$. That is the reason why the contact peaks of the neutral system are so high. Hence, at these volume fractions, the charge correlations in the neighborhood of the macroparticle are masked by the strong steric contributions. Notwithstanding, we remark that, for barely charged systems, the absolute values of the ionic RDFs close to the surface and the extent of their deviations with respect to the pure hard-sphere mixture will rule the behavior of the IC and MEP and, as it is evidenced below, will be crucial to the degree of appearance of CR and OC.

The adequacy of a theoretical description of the present EDL systems will depend on its ability to capture correctly the electrostatic and steric correlations close to the macroparticle. In this regard, the integral equations results portrayed in Fig. 1 illustrate that HNC/MSA follows closely the trends of the simulations, with quantitative discrepancies near the colloid where this scheme overestimates the RDFs. In contrast, the URMGC data exhibit very different tendencies from those of the simulations. Especially noticeable is the pronounced separation between the URMGC radial distribution function of small ions and those from HNC/MSA and Monte Carlo, as well as the very low values of the URMGC normalized density of cations in the zone comprised by the Helmholtz planes. In fact, such exaggerated absence of small ions in URMGC will be of consequence in our later analysis of charge reversal and overcharging. Also, and contrary to the MC data, the URMGC theory predicts $g(r)$ s that are monotonic beyond the OHP, a well documented charac-

teristic of point-ions theories [2, 4, 68]. From the previous discussion, it is therefore expected that the ensuing properties of the EDL extracted from the HNC/MSA and URMGC ionic profiles should present important discrepancies, with HNC/MSA excelling in the comparison with Monte Carlo.

To better visualize the distribution of charge around the neutral macroparticle, let us focus on the function $\rho^*(r)$. The analysis of the inset of Fig. 1 shows that the Monte Carlo LECD around the colloid exhibits a structure with alternating domains of positive and negative local charge. Three intervals are clearly seen in the scale of the graph. The first domain is positive and encompasses the region between the Helmholtz planes. A second space, where $\rho^*(r)$ is negative, spans from the OHP up to $r'/D_+ \approx 2.4$, and a third interval, where $\rho^*(r) > 0$, is located at $2.4 \lesssim r'/D_+ \lesssim 3.4$. In the first domain the local charge is positive because the larger ionic species (the anions) is completely excluded from this region. Beyond the OHP $\rho^*(r')$ drops sharply to a large negative value, due to the presence of a compact contact layer of anions at the OHP. The charge remains negative in this second region until the concentration of positive and negative ions equalize, namely at the first crossing point of the corresponding radial distribution functions. Clearly in the third zone the population of cations dominates, leading to the positive charge observed in the graph. This pattern of alternating domains continues as one goes away from the surface of the macroion, although they are not distinguishable in the scale of the figure. Again, we should note that HNC/MSA parallels very nicely the MC simulations, whereas URMGC predicts a monotonic, asymptotic increase of the local charge outside the Helmholtz planes. Thus, for the last theory, the charge outside the Helmholtz planes, at any distance from the macroion, is always dominated by the anions, which departs evidently from the predictions of Monte Carlo and HNC/MSA.

Complying with the behavior of the local charge, and given that $\frac{dP(r')}{dr'} = \rho^*(r')$ (see Eq.(7)), the $P(r')$ variates as it is observed in Fig. 2 (main panel). Interestingly, we note that all the simulational and theoretical IC curves present the adsorption of a layer of charge very close to the macroion's surface; such layer begins at the IHP and reaches its maximum value of charge at the OHP. The amount of charge in the Helmholtz zone is significant ($\approx 3.8e, 4.1e$ and $2.2e$ for MC, HNC/MSA and URMGC, respectively) and, in turn, gives rise to the formation of a double layer beyond the OHP (see Fig. 1). The existence of this zero surface charge double layer (ZSC-DL) in our calculations is regarding since confirms the ideas originally proposed by Dukhin et al. [34] and, in addition, agrees with previous studies of the ZSC-DL in planar geometry via Monte Carlo simulations [51], and the URMGC and density functional theories [44, 53]. In the MC and HNC/MSA cases, after its maximum, the IC decreases until changing sign and, subsequently, exhibits a region of negative values for $1.8 \lesssim r'/D_+ \lesssim 3.0$. Far-

ther than $r'/D_+ = 3.0$ the accumulated charge fluctuates around zero and, finally, the electroneutrality condition is obtained when $r' \rightarrow \infty$. Contrarily, the $P(r')$ of URMGC goes uniformly to zero.

The information presented so far clearly evince that, at the point of zero charge, a very simple 1:1 salt in contact with a macroparticle already displays highly nonlinear effects such as charge adsorption (i.e. a ZSC-DL) or the reversion in the sign of the IC. These phenomena are due to both the finite ionic size and to the asymmetry between the electrolytic species of the model. Since HNC/MSA fully incorporates such conditions, it is able to reproduce all the characteristics observed in the simulations, even at a quantitative level. In contrast, URMGC does not embody completely the ionic size correlations, just the non-zero contact distances between the colloid and ions. This is enough to capture the adsorption of charge, but not the additional traits of the accumulated charge at intermediate and large r' . In particular, URMGC fails to detect the sign reversal in $P(r')$, predicting instead a monotonic neutralization of the effective charge adsorbed inside the Helmholtz planes. In other words, the partial inclusion of the ionic size and size asymmetry contributions in URMGC has the severe inconvenience that, in this semi-punctual approach, the occurrence of steric-related peculiarities, such as the ZSC-DL, charge reversal and the oscillation of the RDFs and IC, is restricted exclusively to the region between the Helmholtz planes. This fact, to which we will refer to as *the localization of the size and asymmetric effects in URMGC*, will be a recurrent issue in our posterior discussions of the MEP and overcharging.

The mean electrostatic potential as a function of the distance to the uncharged macroparticle is plotted in the inset of Fig. 2. The first thing worth to be noticed is that, despite a zero charge on the colloid, the MC, HNC/MSA and URMGC mean electrostatic potentials at the IHP are positive. This potential of zero charge (PZC) has been largely recognized as a direct consequence of the ionic size asymmetry in the EDL since the initial papers by Valleau and others [44, 45] and, in the mean time, it has received great attention in diverse simulation and theoretical accounts of the planar double layer [50, 51, 53]. Evidently, this PZC is due to the dominant population of cations close to the macroion. Far from the surface of the macroion the MEP of MC and of HNC/MSA tend to zero, but for intermediate distances they have a series of minima and maxima of alternating sign. In particular, the first minimum defines the region where the MEP reversal is stronger. Now, if the wanted association between the electrokinetic and mean electrostatic potentials is invoked [4], the mentioned comportment of the MEP suggests that a macroparticle could experience electrophoresis, even if it is uncharged. Thence, for small cations and depending on the precise localization of the slipping surface [68], the neutral colloid should move in the direction of the applied field if this surface is somewhere in between the Helmholtz planes, or back-

wards if the shear boundary is around the first minimum. It is generally accepted that the slipping or ζ -plane is very close to the surface of the macroions [68], therefore we expect the first scenario to be more plausible. Note that URMGC foresees that the macroions should flow always in the direction of the external electric field.

So far we have examined systems at the point of zero charge, where no electrostatic correlations between the macroparticles and the surrounding ions were considered. In spite of that, the colloid-ion entropic contributions and the inter-ionic correlations led to interesting phenomena. By weakly charging the macroions, conspicuous effects such as charge reversal and overcharging now arise, as it is seen in the remaining of this section. Then, let us evaluate two situations in which the valence of the macroion is $z_M = -4$ and $z_M = 4$ (i.e. surface charge densities $\sigma = \pm 0.051 \text{ C/m}^2$), immersed in the same 1:1 electrolyte as before. Note that by virtue of z_M the role of anions and cations as counterions or coions is interchanged. Fig. 3 includes the radial structure (main panel) and the local charge (insets) of the electrolyte around the macroion for the two values of z_M . Fig. 3a contains the case in which the counterions are smaller than the coions ($z_M = -4$), whereas the case of larger counterions ($z_M = 4$) is reported in Fig. 3b. Fig. 3a reveals that, compared to the RDFs of a neutral macroparticle in Fig. 1, the presence of the counterions in MC and HNC/MSA is greater when the surface is negatively charged, as evidenced by the increased contact peak, whereas the concentration of coions diminishes. This fact stresses the relevance of charge correlations (induced by z_M) on the ordering of the ions around the macroparticle. Clearly, the RDFs of URMGC disagree with MC and HNC/MSA. On the other hand, for $z_M = 4$ (counterions larger than coions, Fig. 3b), we see a dramatic decrement in the contact peak of the smaller ions (coions) and an augment in that of the larger ions (counterions), which is adequately reproduced by HNC/MSA and not by URMGC. Since we are dealing with charged systems, size and charge correlations are into play. As a result, these two cases produce LECD functions that look very different (see the insets of Fig. 3). In addition, both insets show that the local charge profiles of simulation and HNC/MSA exhibit a sequence of positive and negative regions. Quantitatively, however, the first positive zone is much more pronounced for $z_M = -4$, whereas for $z_M = 4$ the second and third domains are much more important. In particular, it is worth to notice that, for simulation and theories, the first region is positive in the two cases, even if the charge of the macroion is positive, which indicates that, for $z_M > 0$, this first layer, rather than to screen the bare charge of the macroion, it emphasizes such native charge, which is a remarkable effect induced by the smaller size of the coions.

Further details can be grasped by looking at the $P(r')$ curves, as they are presented in Fig. 4. For $z_M = -4$ (Fig. 4a) we find that the Monte Carlo IC increases almost linearly inside the Helmholtz planes, inverting

its original sign (*i.e.* *experiencing charge reversal*) and reaching a maximum of $P_{max}(r') \approx 1.3$ at the OHP. After the OHP, $P(r')$ acquires a fluctuating behavior, where subsequent charge inversions can be appreciated. The inset of the figure indicates that the mean electrostatic potential is also oscillatory, with a maximum inversion inside the Helmholtz zone. The level of accuracy of the theories can be readily estimated from the figure and its inset. Particularly, we see that, differently from HNC/MSA, URMGC is unable to describe any reversal of the accumulated charge or the mean electrostatic potential throughout all the space. This represents an extreme manifestation of the so-called localization of the size and asymmetric effects in URMGC.

The functions $P(r')$ and $\psi(r')$ for $z_M = 4$ are portrayed in Fig. 4b and its inset. Notably, the Monte Carlo $P(r')$ *increases* in between the Helmholtz planes, revealing an *adsorption of charge of the same sign as that of the macroion*, which in turn “augments” the native macroion charge up to a maximum value of $P_{max}(r') \approx 6.3$ at the OHP. This striking event is referred to as *overcharging*. Overcharging (OC) was predicted theoretically by Jiménez-Ángeles and Lozada-Cassou [23] for a charged wall in contact with a mixture of macroions and a fully-symmetric salt. To this date, this peculiarity had not been confirmed through simulations or experiments. Hence, our results provide the first simulational evidence of OC in a very simple model, where such “anomaly” is a direct consequence of the ionic size asymmetry when charge correlations are not too strong, *i.e.* close to the point of zero charge. In this sense, overcharging appears when size correlations dominate over charge correlations near the point of zero charge. This implies, therefore, that OC is also expected in other geometries, whenever ionic size asymmetry is present. We would like to point out that the results presented here are in line with our previous reports [5, 54], where it has been established that the properties of the electric double layer depend on the two species of a binary electrolyte, and not only on the counterions as it has been widely accepted. On the other hand, regarding the performance of the theoretical schemes we are working with, we realize that URMGC is capable to describe the overcharging, but not the oscillations and the charge reversal observed in the MC data, nor the inversion of the corresponding MEP. This fact is a typical expression of the URMGC restraint of all the excluded volume and size asymmetry phenomena to occur exclusively in the Helmholtz zone. Contrastingly, HNC/MSA collates very well with the simulational data, describing correctly all these characteristics.

To analyze the behavior of the integrated charge as we depart from the point of zero charge, in Fig. 5 we present $P(r')$ of MC and HNC/MSA for two sequences in z_M . When counterions are smaller than coions ($z_M < 0$, Fig. 5a), the maximum simulational charge reversal observed at the OHP decreases as the valence of the macroion becomes more negative. In fact, charge reversal within the Helmholtz planes disappear altogether for $z_M \approx -7$. For

$z_M < -7$ the first layer of charge reversal shifts further away from the macroparticle. On the other hand, in the curves corresponding to coions smaller than counterions ($z_M > 0$, Fig. 5b) overcharging occurs, and the difference between the peak of overcharging (at the OHP) and z_M (at the surface) decreases as z_M increases, which is the result of the growing macroion-coions repulsion. Overcharging virtually disappears everywhere when this electrostatic repulsion becomes strong enough, which for this system corresponds to $z_M \approx 24$. Consequently, the maximum of overcharging only happens at the OHP, indicating that it is a feature directly caused by the size asymmetry of the ions in a binary electrolyte. From Fig. 5 the good coincidence between the simulations and the HNC/MSA theory is manifest.

A more careful inspection of the Monte Carlo IC graphs when $z_M < 0$ (see the inset of Fig. 5a) shows that, at least for short distances, the profiles seem to cross each other at specific points, defining in this way intervals where the integrated charge as a function of z_M follows a regular pattern, as we explain next. Thus, for instance, $0 \leq r'/D_+ \lesssim 1.6$ (note the upward arrow in the figure) delimits a region where, for fixed r' , the simulated IC decreases when z_M diminishes. HNC/MSA exhibits the same trend for $0 \leq r'/D_+ \lesssim 1.55$ (downward arrow). The next crossing point of the charge profiles determines another space where, for a given position, the IC now *augments* when z_M decreases. For simulations this occurs in the interval $1.6 \lesssim r'/D_+ \lesssim 2.9$ (upward arrow), and in $1.55 \lesssim r'/D_+ \lesssim 3.1$ for HNC/MSA (downward arrow). Below, we will return to explore the relevance of these findings. Previously, we proceed to consider the $P(r')$ in URMGC.

The integrated charge of URMGC does not follow any of the aforesaid tendencies. In the first place, for $z_M < 0$ (Fig. 6a), such theoretical approach exhibits charge reversal only for a colloidal charge of $z_M = -2$ and this reversal is weak ($P_{max}(r') \approx 0.7$ at the OHP), which means that, differently from Monte Carlo and HNC/MSA, the CR disappears already for $z_M < -2$. The origin of this comportment of the CR can be traced back to the very low values of the URMGC concentration of small cations near a discharged surface reported in the main panel of Fig. 1. When the negative charge on the initially neutral colloid starts to grow (*i.e.* z_M becomes more negative), the small (and positive) counterions are attracted to the macroparticle and increase their number in the Helmholtz zone, then producing charge reversal for very low z_M ($-2 \lesssim z_M < 0$, for URMGC). However, due precisely to the mentioned URMGC scarcity of small counterions at $z_M = 0$, the growth of the negative surface charge overtakes that of the charge reversal owed to the counterions, and rapidly suppresses it. Secondly, and in further contrast with MC and HNC/MSA, in the data of Fig. 6a we notice that, once the reversal of charge in URMGC ceases to occur in the Helmholtz region (for $z_M \lesssim -2$), it is never observed again at any point beyond the OHP in the monotonically decreasing profiles

of $P(r')$. Evidently, this is another example of the localization of the ionic size and size asymmetry effects in the semi-punctual URMGC formalism. Complementarily, for $z_M > 0$ (Fig. 6b), the URMGC integrated charge presents overcharging within the Helmholtz planes, which diminishes slowly as z_M augments. Notwithstanding, the OC in this theory is less important than that in simulations and HNC/MSA, as can be verified from a comparison of the respective differences $|P(r') - z_M|$. Besides, and as expected, the IC curves in Fig. 6b go uniformly to zero after the OHP. Such abatement of the overcharging in URMGC for positive surface charges can also be explained in terms of the low presence of small ions close to a discharged macroparticle. In this case, when the positive colloidal charge is being incremented from the zero value, the shortage of small cations (coions) available to build-up the overcharging in the proximities of the surface lessens the magnitude of the anomalous effect.

On the other hand, apart from the usual monotonicity of the URMGC integrated charge as a function of the distance, in the two sequences of curves for different z_M presented in Fig. 6, we observe an extra monotonic character of the $P(r')$ profiles, this time with respect to the variation of z_M . Specifically, in Figs. 6a and 6b the IC curves associated to distinct values of z_M never cross each other. Thus, we find that the URMGC integrated charge functions, for any fixed r' , satisfy the condition

$$\frac{\partial P(\sigma_0, r')}{\partial \sigma_0} > 0. \quad (11)$$

Otherwise, and as it was prefigured in relation with the inset of Fig. 5a, the integrated charges of MC and HNC/MSA show regions where the alternative condition

$$\frac{\partial P(\sigma_0, r')}{\partial \sigma_0} < 0 \quad (12)$$

is satisfied. We realize that this last ‘‘anomalous’’ behavior is possible due to the presence of crossing points in the corresponding IC profiles. Physically, Eq. (11) establishes that if the charge over the macroion is increased, the corresponding effect in the spherical EDL is to augment locally the IC, which is intuitively awaited. Contrastingly, Eq. (12) states that the enlargement of the macroion’s charge promotes a local decrease in the IC. We refer to this behavior as a *local inversion of derivative of the integrated charge* (LIDIC). It should be noted that such inversion of the derivative occurs only when $z_M < 0$. This same phenomenon seems to be absent for MC and HNC/MSA if $z_M > 0$ (see Fig. 5b) and, instead, it is apparent that all the IC profiles meet at their first minimum ($r'/D_+ \approx 2.3$).

In order to explore the behavior of the potential-charge relationship in the SEDL, the simulational and theoretical mean electrostatic potentials at the Helmholtz planes as functions of σ_0 are plotted in Fig. 7. As it is usual in the analysis of the $\psi_{IHP}(\sigma_0)$ and $\psi_{OHP}(\sigma_0)$ functions,

the colloidal charge is specified here in terms of the surface density $\sigma_0 (= z_M e / (\pi D_M^2))$. The reader can easily pass from σ_0 to z_M if realizes that the symbols (open circles) in the figure correspond to the sequence of integer valences $z_M = -8, -6, -4, -2, 0, +2, +4, +6, +8$. In Figs. 7a and 7b, we observe that the $\psi_{IHP}(\sigma_0)$ and $\psi_{OHP}(\sigma_0)$ curves for the three approaches, namely Monte Carlo, HNC/MSA and URMGC, display an increasing monotonic behavior and positive potentials of zero charge (PZCs). Besides, the simulations and theories predict *the existence of intervals of negative colloidal charges, near the point of zero charge, for which the potentials at the IHP and OHP can be positive*, i.e. where the conditions $\psi_{IHP}\sigma_0 < 0$ and $\psi_{OHP}\sigma_0 < 0$ are accomplished. As it is indicated by Eq. (8), these attributes of ψ_{IHP} and ψ_{OHP} can be inferred, of course, from the comportment of the integrated charge, or better from the function $P(r)/r^2$ (which is basically the local mean electrostatic field around the macroparticle). To facilitate our argument let us start with the case of the URMGC theory. In Fig. 2 we found that, for an uncharged colloid, $P(r') \geq 0$ for all r' in the URMGC scheme. Therefore, from the definition of the MEP (Eq. (8)), it follows that $\psi(r')$ must be positive at any distance from the neutral surface; in particular, the relations $\psi_{IHP} > 0$ and $\psi_{OHP} > 0$ hold. This explains the positive URMGC PZCs at the IHP and OHP. Moreover, the series of IC curves graphed in Fig. 6 show a uniform precedence with respect to the variation of σ_0 , or that $P(r', \sigma_0) > P(r', \sigma'_0)$ if $\sigma_0 > \sigma'_0$. We can state this equivalently by saying that there are not LIDIC regions in the sequence of curves in Fig. 6. This necessarily implies that $\psi(r', \sigma_0) > \psi(r', \sigma'_0)$ at any distance from the neutral macroparticle, which elucidates the monotonically increasing behavior of the ψ_{IHP} and ψ_{OHP} for URMGC noticed in Fig. 7. This same precedence of $P(r', \sigma_0)$ with respect to σ_0 signifies that, at a fixed distance from the macroparticle, there must be a σ_0^{crit} for which $\psi(r', \sigma_0^{crit}) = 0$. Given that in the URMGC formalism such σ_0^{crit} happens for both the IHP and OHP potentials within the range plotted in the figure, we thus find negative values of σ_0 , close to the point of zero charge, associated to positive values of ψ_{IHP} and ψ_{OHP} .

The properties of the $\psi_{IHP}(\sigma_0)$ and $\psi_{OHP}(\sigma_0)$ obtained from Monte Carlo and HNC/MSA can be analyzed using similar ideas to those just applied to URMGC. The task is more complex, however, because $P(r)/r^2$ is an alternating function for both the simulations and HNC/MSA, which would require a more detailed examination of the positive and negative areas involved in the evaluation of Eq. (8). Fortunately, such process can be clarified if we note that: (i) in Fig. 2 the ICs of MC and HNC/MSA for a neutral colloid have a very high positive peak centered at the OHP, which contributes more than the adjacent minimum at $r' \approx 2.4$ to the integral of $P(r)/r^2$ when ψ_{IHP} and ψ_{OHP} are being calculated, and (ii) that precisely these first maximum and minimum in $P(r')$ dominate the integrals associated to ψ_{IHP} and ψ_{OHP} (ψ_{IHP} -integral and ψ_{OHP} -integral, respectively).

From (i) and (ii) the positive sign of the Monte Carlo and HNC/MSA PZCs then arises. The recognition of the determinant role that the first extrema in the ICs have for the evaluation of ψ_{IHP} and ψ_{OHP} is very important since it provides the key to understand the complete shape of the $\psi_{IHP}(\sigma_0)$ and $\psi_{OHP}(\sigma_0)$ coming from MC and HNC/MSA. The rationale proceeds as follows. Differently from URMGC, in Figs. 5a and 5b the sequences of ICs of simulation and HNC/MSA for distinct colloidal charges are non-monotonic with respect to r' and display LIDIC regions (Fig. 5a). Notwithstanding, in Fig. 5b it can be seen that, for $\sigma_0 > 0$, the height of the overcharging peak at the OHP increases when σ_0 augments, or else that the fact (i) of the previous paragraph occurs in a more emphatic way as σ_0 heightens. Consequently, such enhancement of (i), combined with the prevailing fact (ii), results in the increasing behavior of $\psi_{IHP}(\sigma_0)$ for positive σ_0 observed in simulations and HNC/MSA. Otherwise, for $\sigma_0 < 0$, it is better to consider the OHP as a reference point to split the contributions of $P(r')$ to the ψ_{IHP} -integral. In this form, it can be seen that, for $\sigma_0 \lesssim -0.051 \text{ C/m}^2$ ($z_M \lesssim -4$), the area comprised by that section of the IC before the OHP becomes more negative, and more important than the area enclosed by the IC beyond the OHP, when σ_0 decreases. Thus, such argument explicates the increasing comportment of $\psi_{IHP}(\sigma_0)$ for negative σ_0 , as well as the existence in Monte Carlo and HNC/MSA of an interval of negative surface charges for which ψ_{IHP} is positive. With respect to $\psi_{OHP}(\sigma_0)$ in simulations and HNC/MSA, from Fig. 5 it is evident that, for those 1:1 systems, the value (and sign!) of the ψ_{OHP} -integral is determined by overcharging, for $\sigma_0 > 0$, and by charge reversal, for $\sigma_0 < 0$. For positive colloidal charges, the increment of the height of the overcharging peak at OHP when z_M augments dictates the increasing positiveness of ψ_{OHP} . In addition, we notice that, for negative macroparticle charges, a dominant peak of charge reversal occurs either at the OHP or beyond that point, which in the present work is a distinctive feature of those descriptions that incorporate consistently the ionic size and size asymmetry effects (i.e. simulations and HNC/MSA) and, therefore, it is absent in URMGC. Such strong charge reversal gives rise to the positive sign of ψ_{OHP} for negatively charged colloids, and then completes our explanation of the fact that, for simulations and HNC/MSA, ψ_{OHP} is always positive for the range covered in Fig. 7b.

In connection with electrophoresis experiments, and depending on the location of the shear plane, our results suggest two possible scenarios. If the sign of the electrophoretic mobility, μ , were associated to the sign of the potential ψ_{IHP} , our treatment of the size-asymmetric EDL would predict the inversion of the colloidal mobility very near to the point of zero charge. In contrast, if the sign of μ were associated to the sign of the potential ψ_{OHP} , our study would foresee positive mobilities in a wider range of colloidal charges around zero. In addition, Fig. 7b resembles a situation reported in Fig. 2b

of Ref. [38] by Johnson et al., where zeta potential measurements of α -alumina in presence of 1 M LiNO_3 are plotted as a function of pH. In those results, the zeta potential is always positive in a wide interval of pH that encompasses the point of zero charge, which parallels our results in Fig. 7b. This would indicate that such positive values of the zeta potential are due in part by the preferential adsorption of one of the species (Li^+), which in turn should be induced by the ionic size asymmetry, as deduced from our survey of the spherical EDL. Although other complex mechanisms are into play in these kind of experiments [39, 40, 72, 73], our size-asymmetric model seems to capture adequately relevant phenomena occurring in real systems, and hence it could be considered as a basic representation of the EDL to which further improvements (as Van der Waals dispersion forces or more sophisticated chemical mechanisms) can be incorporated in order to predict experimental data more accurately.

B. Divalent size-asymmetric electrolytes

We proceed to investigate the properties of the electrical double layer for a macroion immersed in a 2:2 salt, i.e. for systems with stronger charge correlations. As it will be shown, many of the findings reviewed in the prior section devoted to univalent electrolytes are also present, in an enhanced way, for the case of divalent ions. As before, we examine first the EDL at the point of zero charge and later we ponder instances with charged macroparticles. In what follows, we consider EDL systems formed by a colloid and a bath of a 2:2, 0.5 M electrolyte, with the same diameters as specified in the earlier section.

The simulational, HNC/MSA and URMGC radial distributions of divalent ions around a macroparticle with $z_M = 0$ are included in Fig. 8 (main panel). There we have incorporated the Monte Carlo and HNC/MSA pair correlation functions for the associated hard-sphere mixture (uncharged “ions”). Again, the idea is to exemplify how the coulombic correlations modify the structure of the pure hard-sphere fluid, in order to gain some insight into the relative importance of the entropic and charge correlations. From the direct contrast between the simulational RDFs of hard spheres and ions in the main panel of the figure, we observe that the charge effects are very strong, completely modifying the accumulation of the smaller species around the macroparticle. In fact, the changes in the Monte Carlo $g_j(r')$ of divalent ions with respect to the RDFs of hard spheres are bigger than those occurring in univalent systems (compare the main panels of Figs. 1 and 8). For the simulations of 2:2 electrolytes, the impact of the valence is much more important for the smaller ionic species, where we observe that the corresponding contact population depletes so much that the concentration of cations near the surface is below the bulk value. A similar dewetting has been reported in a recent study of the planar EDL for size-asymmetric 1:1, 1:2 and 1:3 salts [53], with the multiva-

lent ions corresponding to the smaller species. In that work it was found that the amount of small cations in the proximities of a neutral plane decreased as long as the electrostatic coupling (i.e. the valence) was heightened, being our results consistent with such behavior. On the other hand, in Fig. 8 (main panel) we can appreciate that the HNC/MSA results for hard spheres compare well with the simulations, whereas for the divalent case this formalism overestimates the Monte Carlo data for the two ionic species. Furthermore, HNC/MSA fails to describe the correct tendency for the RDF of big anions, predicting an increase of such function with respect to the corresponding RDF of the larger hard spheres, which is clearly not the behavior seen in the MC data. Despite this poor achievement in the estimation of the $g_j(r')$ for the electrolyte, HNC/MSA does well at the level of the local electrolyte charge density (see inset of Fig. 8), capturing the correct trends of the simulations. This is not a surprising circumstance given that the dependence of $\rho^*(r')$ on the difference $g_+(r') - g_-(r')$ explains why the notable discrepancies existing between the RDFs of Monte Carlo and HNC/MSA are attenuated when the local charge densities are compared instead. URMGC, on the other hand, highly disagrees with the simulations for the $g_j(r')$ and $\rho^*(r')$. Special note must be taken of the very low URMGC concentration of small ions in the Helmholtz zone, which, analogously to the univalent case, will determine the weak intensity of the CR and OC phenomena for 2:2 systems in this theory.

The simulational and theoretical ionic distributions of the divalent salt yield the accumulated charge and mean electrostatic potential given in Fig. 9 and its inset. As it was detected in the monovalent situation, the ionic size asymmetry promotes an adsorbed layer of charge and the concomitant existence of a zero surface charge double layer (see Fig. 8), as well as a non-zero MEP at (and between) the Helmholtz planes. The adsorbed charges, up to the OHP, are $\approx 2.6e$, $3.3e$, and $2.0e$ for MC, HNC/MSA, and URMGC, respectively, which are smaller than those observed for the 1:1 salt. In turn, contrasted with Monte Carlo, the MEP within the Helmholtz planes is overestimated by HNC/MSA and underestimated by URMGC. Globally we see that the performance of HNC/MSA and URMGC is very similar to that displayed for the monovalent salt, with a better qualitative similitude between HNC/MSA and the simulations. For URMGC the $P(r')$ and $\psi(r')$ profiles evidence the restriction of all the size asymmetry and hard-core effects to happen uniquely in the Helmholtz zone.

The Monte Carlo and theoretical RDFs, LECD, IC, and MEP curves corresponding to the divalent system and two values of the colloidal charge, namely $z_M = -4$ and $z_M = 4$, are plotted in Figs. 10 and 11. When $z_M = -4$ (Fig. 10a), there is a strong adsorption of counterions inside the Helmholtz planes, accompanied by an important depletion of coions, particularly for MC and HNC/MSA (main panel). Besides, it is worth noticing that very close to the OHP the concentration of coions is

smaller than that of counterions (compare with Fig. 3a), which seems to indicate that at these distances the repulsion forces between the macroion and the coions are far from being screened. The associated local charge densities are portrayed in the inset, where we have curves that do not jump to a negative value immediately after the OHP, showing that the macroion-coions repulsion propagates beyond the Helmholtz planes. When $z_M = 4$ (Fig. 10b), and despite of the intense electrostatic repulsion, the MC, HNC/MSA and URMGC concentrations of the small coions close to the IHP turn out to be small but finite, effectively increasing the charge of the macroion, and therefore driving a significative enhancement in the counterions concentration near the OHP (main panel). As a result, the LECD profiles develop a small first positive layer followed by an ample negative region (see inset).

In Fig. 11 we present the integrated charges and MEPs for the divalent salt and macroion valences $z_M = -4$ and $z_M = 4$. For $z_M = -4$ (panel (a)), the ICs of Monte Carlo and HNC/MSA exhibit charge reversal in the Helmholtz zone, but the maximum charge reversals are outside that region (at $r'/D_+ \approx 1.5$ and $r'/D_+ \approx 1.4$ for simulations and HNC/MSA, respectively). The corresponding MEPs, on the other hand, display a strong reversal, with the maximum potential being inside the Helmholtz planes (see inset). In the case $z_M = 4$ (panel (b)) we see that the MC and HNC/MSA integrated charge profiles present overcharging, followed by alternate oscillations of decreasing amplitude, whereas the associated MEPs (in the inset) decay in a fluctuating manner to zero. This observation of OC in the computer “experiments” of divalent systems complements our previous findings for univalent salts and, thus, consolidates our simulational proof of overcharging as a genuine feature of size-asymmetric primitive model EDLs.

A simultaneous analysis of all the structural information for divalent systems contained in Figs. 10 and 11 show that the HNC/MSA theory follows closely the Monte Carlo data, whereas the URMGC approach exhibits notable differences with respect to the simulations. From these figures it is also verified that in the URMGC description of the EDL there is a confinement of the steric-related phenomenology (e.g. CR, OC and the non-monotonic character of the structural functions) within the Helmholtz zone.

Fig. 12 portrays the Monte Carlo and HNC/MSA integrated charges for varying z_M ($-8 \leq z_M \leq 8$) in order to analyze the evolution of the size asymmetry effects when the divalent systems depart from the point of zero colloidal charge. For $z_M < -2$ (Fig. 12a) the IC profiles of MC and HNC/MSA present charge reversal, with the maximum located outside the Helmholtz zone. As the charge increases (towards $z_M = 0$) the location of the peak of each curve shifts to shorter distances and eventually lands at the OHP. Further increase of z_M leads to the results plotted in Fig. 12b, where the system displays overcharging, with a maximum intensity

(i.e. $|P(r') - z_M|$) that decreases with the augment of the macroion's valence. This overcharging phenomenon only takes place in between the Helmholtz planes, and it is followed by a first region of charge reversal. At the limiting valence $z_M \approx 16$ overcharging virtually disappears; meanwhile the charge reversal beyond the OHP continues to exist with an increasing magnitude. All these characteristics of $P(r')$ for $z_M > 0$ are equally described for both the simulations and HNC/MSA. The complete development of the $P(r')$ for 2:2 electrolytes and $-8 \leq z_M \leq 8$ reveals a passage from charge reversal to overcharging. This crossover at $z_M = 0$ is due uniquely to the size asymmetry of the salt ions, as the change of sign of z_M merely inverts the role of the anions and cations (as coions or counterions).

Therefore, in the present investigation it has been found that the charge reversal and overcharging observed near the point of zero charge are mainly caused by entropic contributions coming from the size-asymmetric nature of the electrolyte ions. However, when z_M is increased, the charge reversal and overcharging in the Helmholtz zone disappear, and only CR persists. This remaining charge reversal beyond the OHP comes from the interplay between excluded volume and electrostatic correlations and, thus, it is not exclusive of a size-asymmetric model. That is the reason why charge reversal has been already reported in many studies of the restricted primitive model EDL, in which the excluded volume effects are also consistently taken into account [74]. Accordingly, EDL theories for genuine punctual ions and uniformly charged surfaces do not predict charge reversal at all.

We would like to mention that our divalent systems also exhibit regions of local inversion of the derivatives of the integrated charge (LIDIC). These zones are delimited in Figs. 12a and 12b by the upward arrows for Monte Carlo and by the downward arrows for HNC/MSA. Inside these ‘‘anomalous’’ regions the accumulated charge at any point decreases when the colloidal charge is augmented and vice versa. Similarly to the univalent case, and starting from the definition of the MEP (see Eq. (8)), the existence of this LIDIC domains provides a way to explain the behavior of the potential-charge relationship at the Helmholtz planes.

The corresponding sequence ($-8 \leq z_M \leq 8$) of URMGC integrated charges for 2:2 electrolytes is given in Fig. 13. Visibly, each one of the profiles in this series varies monotonically with respect to the distance r' and, as a whole, the full set of curves changes monotonically as a function of z_M . In other words, after the OHP, every $P(r')$ goes to zero without spatial oscillations, and the complete sequence does not show LIDIC regions.

The MEP of MC, HNC/MSA, and URMGC at the Helmholtz planes are shown in Fig. 14 as a function of the surface charge σ_0 . At the IHP, all the approaches exhibit a MEP that is monotonic and displays a positive zero-charge potential and a negative σ_0^{crit} such that $\psi_{IHP} > 0$ for $\sigma_0^{crit} < \sigma_0 < 0$, just like in the monovalent

systems. From panel (b) we also find that ψ_{OHP} is also monotonic for URMGC. In contrast to the monovalent case, however, ψ_{OHP} from MC and HNC/MSA is non-monotonic and displays a minimum at a positive σ_0^{min} . This augment of ψ_{OHP} when σ_0 decreases below σ_0^{min} suggests that there could be experimental systems in which the reverted electrophoretic mobility always increases its magnitude.

The trends of these MEPs can be explained in terms of the corresponding IC profiles (see Figs. 12 and 13), as discussed previously in the context of monovalent electrolytes. In particular, the concavity of ψ_{OHP} for MC and HNC/MSA can be explained by observing in Fig. 12b the behavior of the integral of $P(r)/r^2$ between two consecutive electroneutral points of $P(r)$, and noting that the absolute value of these negative areas decreases when z_M diminishes. Thus, for $\sigma_0 \geq 0$, the area from the OHP to the first electroneutral point is positive and larger than the negative area between the first and second electroneutral points (see Fig. 12b). Since the difference between these two contributions to the ψ_{OHP} increases with σ_0 , this explains the positive value of ψ_{OHP} and its increasing behavior. An analogous argument explains the trends observed when $\sigma_0 < 0$ (Fig. 12a), despite the disappearance of the maximum charge reversal at the OHP when z_M decreases.

The concavity of ψ_{OHP} can also be cast in terms of the *local inversion of derivative of the MEP* (LIDMEP), which we define analogously to the LIDIC. With this in mind, Fig. 15 shows the MEP of the divalent system for several values of z_M . For $z_M < 0$ the MC data shows a region of LIDMEP in $0.82 \lesssim r'/D_+ \lesssim 2.6$ (upward arrows in Fig. 15a). A similar region is seen in Fig. 15b ($z_M > 0$). The downward arrows in these figures indicate the location of such regions for HNC/MSA. Therefore, the change in sign of the derivative of the MEP observed in Fig. 14b appears because the OHP is in a LIDMEP region, where

$$\frac{\partial \psi(\sigma_0, r' = D_+)}{\partial \sigma_0} < 0. \quad (13)$$

Since ionic size and size asymmetry are evidently important in real highly coupled electrokinetic systems, these last results suggest that the interpretation of the zeta potential ζ in electrokinetic experiments must be done carefully because the experimental MEP profiles could present LIDMEP regions, according to our model calculations. Consequently, the measured ζ might correspond to potentials located in LIDMEP regions, giving rise to the possibility of decreasing ζ for increasing σ_0 and vice versa. The occurrence of these non-monotonic effects in the potential are clearly precluded in the PB-based interpretation of the experimental measurements, as evidenced in the present study.

V. SUMMARY AND CONCLUSIONS

In this paper the size-asymmetric electrical double layer (EDL) of 1:1 and 2:2 salts around a slightly charged spherical macroparticle was studied by assuming the primitive model of an electrolyte as a representation of the ionic bath, and using Monte Carlo simulations and the HNC/MSA integral equation in order to calculate the corresponding properties of the model system. Therefore, in the simulation and HNC/MSA integral equation the important ionic size and size asymmetry effects have been fully incorporated through the consistent consideration of the colloid-ions and ion-ion interactions. Additionally, the possible consequences of a partial treatment of such excluded volume and size asymmetry contributions in the properties of the spherical EDL were assessed via the comparison with the predictions of the classic URMGC theory for spherical geometry. In the semi-punctual URMGC formalism the finite nature of the ions is considered only through the use of two different distances of closest approach between the colloid and counterions and colloid and coions. Our Monte Carlo data evince that the finite size and size asymmetry of the ionic species near a barely charged colloid produce remarkable phenomena, such as charge reversal, overcharging, the existence of potentials of zero charge, and of a zero charge electrical double layer, as well as the possibility of oscillations in the ionic densities, and of sign alternancy in the mean electrostatic potential. The simulations also show that the extent of all these features is intimately linked to the ability of the smallest ions to penetrate the Helmholtz zone. Importantly, in this report we present the first simulational corroboration of overcharging (i.e. of the increment of the native colloidal charge prompted by an anomalous adsorption of coions), a peculiarity originally predicted by Jiménez-Ángeles et al. [23] in a more complex EDL system. Here it is evidenced that, close to the point of zero charge, overcharging is a direct consequence of the size asymmetry of the ions. On the whole, the HNC/MSA results coincide with the simulations, then providing an essentially correct picture of the size-asymmetric SEDL near the point of zero charge. In contrast, URMGC disagrees quantitatively and qualitatively with the Monte Carlo trends in most of the situations examined here. Notably, and due to its inconsistent treatment of the hard-core and electrostatic correlations, URMGC exhibits a spatial localization of all its ionic size and size asymmetry effects within the zone delimited by the inner and outer Helmholtz planes. One of the most characteristic sequels of the full incorporation

of the ionic correlations in all the extension of the EDL, and not only in the Helmholtz zone, is the occurrence of a non-monotonic behavior in the ionic concentration, charge density and mean electrostatic potential profiles of Monte Carlo and HNC/MSA. In this respect, the existence of spatial regions in which the integrated charge and mean electrostatic potential present a non-uniform compartment with respect to the variation of the colloidal charge proves its relevance for the understanding of the potential-charge relationship at the Helmholtz planes. In particular, such “non-uniform” regions serve to explain the existence of a singular minimum in the $\psi_{OHP} - \sigma_0$ curve.

The plausible identification between the well-known zeta potential and the mean electrostatic potential around the Helmholtz zone, which is a usual hypothesis in the interpretation of electrophoretic mobility measurements, leads us to suggest several phenomena (e.g. the presence of an anomalous sign in the zeta potential and the occurrence of increased reversed mobilities) which could be the objectives of future experimental protocols. As a first attempt in this direction, we have pointed out the consistency between our results and some experimental data of electrokinetic mobilities for α -alumina particles. The eventual confirmation in the laboratory of any of the theoretical predictions presented in this work (for example, charge reversal and overcharging) by means of some electrokinetic or static technique could indicate the pertinence of our simple primitive-model-based representation of the size-asymmetric spherical EDL as a starting point to develop more faithful descriptions of real colloidal systems, either in equilibrium or under external fields. Finally, and in relation with this, the rich phenomenology discussed in the present communication, that arises from both the ionic size and size asymmetry effects, puts a word of caution about the possible usage of the Poisson-Boltzmann viewpoint and other contingent formalisms, such as the so-called standard electrokinetic model [75], outside their range of applicability.

Acknowledgments

This work was supported by Consejo Nacional de Ciencia y Tecnología (CONACYT, México), through grants CB-2006-01/58470 and C01-47611, and PROMEP. E. G.-T. thanks CNS-IPICYT for computing facilities, and G. I. G.-G. acknowledges postdoctoral fellowships from CONACYT and Instituto Mexicano del Petróleo.

-
- [1] S. L. Carnie and G. M. Torrie, *Adv. Chem. Phys.* **56**, 141 (1984).
 [2] P. C. Hiemenz and R. Rajagopalan, *Principles of Colloid and Surface Chemistry* (Marcel Dekker, New York,

- 1997).
 [3] H.-J. Butt, K. Graf, and M. Kappl, *Physics and Chemistry of Interfaces* (Wiley-VCH, Darmstadt, 2006).
 [4] R. J. Hunter, *Foundations of Colloid Science* (Clarendon,

- Oxford, 1987).
- [5] G. I. Guerrero-García, E. González-Tovar, M. Lozada-Cassou, and F. de J. Guevara-Rodríguez, *J. Chem. Phys.* **123**, 034703 (2005).
 - [6] M. Elimelech and C. R. O'Melia, *Environ. Sci. Technol.* **24**, 1528 (1990).
 - [7] A. Martín-Molina, M. Quezada-Pérez, F. Galisteo-González, and R. Hidalgo-Álvarez, *J. Chem. Phys.* **118**, 4183 (2003).
 - [8] M. Quesada-Pérez, E. González-Tovar, A. Martín-Molina, M. Lozada-Cassou, and R. Hidalgo-Álvarez, *Colloids and Surfaces A* **267**, 24 (2005).
 - [9] K. Besteman, M. A. G. Zevenbergen, H. A. Heering, and S. G. Lemay, *Phys. Rev. Lett.* **93**, 170802 (2004).
 - [10] K. Besteman, M. A. G. Zevenbergen, and S. G. Lemay, *Phys. Rev. E* **72**, 061501 (2005).
 - [11] F. H. J. van der Heyden, D. Stein, K. Besteman, S. G. Lemay, and C. Dekker, *Phys. Rev. Lett.* **96**, 224502 (2006).
 - [12] B. I. Shklovskii, *Phys. Rev. E* **60**, 5802 (1999).
 - [13] S. L. Carnie, D. Y. C. Chan, D. J. Mitchell, and B. W. Ninham, *J. Chem. Phys.* **74**, 1472 (1981).
 - [14] M. Lozada-Cassou, R. Saavedra-Barrera, and D. Henderson, *J. Chem. Phys.* **77**, 5150 (1982).
 - [15] V. Vlachy and D. A. McQuarrie, *J. Chem. Phys.* **83**, 1927 (1985).
 - [16] E. Gonzales-Tovar, M. Lozada-Cassou, and D. Henderson, *J. Chem. Phys.* **83**, 361 (1985); *ibid.* **87**, 5581 (1987).
 - [17] E. González-Tovar and M. Lozada-Cassou, *J. Phys. Chem.* **93**, 3761 (1989).
 - [18] M. Lozada-Cassou and E. Díaz-Herrera, *J. Chem. Phys.* **92**, 1194 (1990).
 - [19] P. Attard, *Adv. Chem. Phys.* **92**, 1 (1996).
 - [20] H. Greberg, R. Kjellander, and T. Akesson, *Mol. Phys.* **92**, 35 (1997).
 - [21] R. Messina, E. González-Tovar, M. Lozada-Cassou, and C. Holm, *Europhys. Lett.* **60**, 383 (2002).
 - [22] J. Lyklema, *Colloids and Surfaces A* **291**, 3 (2006).
 - [23] F. Jiménez-Ángeles and M. Lozada-Cassou, *J. Phys. Chem. B* **108**, 7286 (2004).
 - [24] E. González-Tovar and M. Lozada-Cassou, *Mol. Phys.* **74**, 367 (1991).
 - [25] M. Lozada-Cassou, in *Fundamentals of Inhomogeneous Fluids*, edited by D. Henderson (Marcel Dekker, New York, 1992).
 - [26] L. Yeomans, S. E. Feller, E. Sánchez, and M. Lozada-Cassou, *J. Chem. Phys.* **98**, 1436 (1993).
 - [27] M. Deserno, F. Jiménez-Ángeles, C. Holm, and M. Lozada-Cassou, *J. Phys. Chem. B* **105**, 10983 (2001).
 - [28] E. González-Tovar, F. Jiménez-Ángeles, R. Messina, and M. Lozada-Cassou, *J. Chem. Phys.* **120**, 9782 (2004).
 - [29] Y. X. Yu, J. Z. Wu, and G. H. Gao, *J. Chem. Phys.* **120**, 7223 (2004).
 - [30] L. B. Bhuiyan, C. W. Outhwaite, and D. Henderson, *J. Chem. Phys.* **123**, 034704 (2005).
 - [31] F. Jiménez-Ángeles, R. Messina, C. Holm, and M. Lozada-Cassou, *J. Chem. Phys.* **119**, 4842 (2003).
 - [32] F. Jiménez-Ángeles, G. Odriozola, and M. Lozada-Cassou, *J. Chem. Phys.* **124**, 134902 (2006).
 - [33] T. Goel and C. N. Patra, *J. Chem. Phys.* **127**, 034502 (2007).
 - [34] A. Dukhin, S. Dukhin, and P. Goetz, *Langmuir* **21**, 9990 (2005).
 - [35] S. S. Dukhin and A. E. Yaroschuck, *Kolloidn. Zh.*, **44**, 884 (1982).
 - [36] B. V. Derjaguin, S. S. Dukhin, and A. E. Yaroschuck, *J. Colloid Interface Sci.* **115**, 234 (1987).
 - [37] S. S. Dukhin, N. V. Churaev, V. N. Shilov, and V. M. Starov, *Adv. Chem. USSR* **43**, 6 (1988).
 - [38] S. B. Johnson, P. J. Scales, and T. W. Healy, *Langmuir* **15**, 2836 (1999).
 - [39] S. B. Johnson, G. V. Franks, P. J. Scales, and T. W. Healy, *Langmuir* **15**, 2844 (1999).
 - [40] M. Colic, G. V. Franks, M. L. Fisher, and F. F. Lange, *Langmuir* **13**, 3129 (1997).
 - [41] R. Rahnemaie, T. Hiemstra, and W. H. van Riemsdijk, *J. Colloid Interface Sci.* **293**, 312 (2006).
 - [42] T. Hiemstra and W. H. Van Riemsdijk, *J. Colloid Interface Sci.* **301**, 1 (2006).
 - [43] M. Manciu and E. Ruckenstein, *Advances in Colloid and Interface Sci.* **105**, 63 (2003).
 - [44] J. P. Valteau and G. M. Torrie, *J. Chem. Phys.* **76**, 4623 (1982).
 - [45] L. B. Bhuiyan, L. Blum, and D. Henderson, *J. Chem. Phys.* **78**, 442 (1983).
 - [46] J. J. Spitzer, *J. Colloid Interface Sci.* **92**, 198 (1983).
 - [47] A. F. Khater, D. Henderson, L. Blum, and L. B. Bhuiyan, *J. Phys. Chem.* **88**, 3682 (1984).
 - [48] U. Marini Bettolo Marconi, J. Wiechen, and F. Forstmann, *Chem. Phys. Lett.* **107**, 609 (1984).
 - [49] C. W. Outhwaite and L. B. Bhuiyan, *J. Chem. Phys.* **84**, 3461 (1986).
 - [50] H. Greberg and R. Kjellander, *J. Chem. Phys.* **108**, 2940 (1998).
 - [51] M. Valiskó, D. Henderson, and D. Boda, *J. Phys. Chem. B* **108**, 16548 (2004).
 - [52] M. Valiskó, D. Boda, and D. Gillespie, *J. Phys. Chem. C* **111**, 15575 (2007).
 - [53] D. Gillespie, M. Valiskó, and D. Boda, *J. Phys.: Condens. Matter* **17**, 6609 (2005).
 - [54] G. I. Guerrero-García, E. González-Tovar, M. Chávez-Páez, and M. Lozada-Cassou, in preparation.
 - [55] G. M. Torrie and J. P. Valteau, *J. Phys. Chem.* **86**, 3251 (1982).
 - [56] D. Boda, W. R. Fawcett, D. Henderson, and S. Sokolowski, *J. Chem. Phys.* **116**, 7170 (2002).
 - [57] L. B. Bhuiyan and C. W. Outhwaite, *Phys. Chem. Chem. Phys.* **6**, 3467 (2004).
 - [58] J. Yu, G. E. Aguilar-Pineda, S.-H. Dong, and M. Lozada-Cassou, *J. Colloid Interface Sci.* **295**, 124 (2006).
 - [59] R. Messina, *J. Chem. Phys.* **127**, 214901 (2007).
 - [60] G. M. Torrie, J. P. Valteau, and C. W. Outhwaite, *J. Chem. Phys.* **81**, 6296 (1984).
 - [61] D. A. McQuarrie, *Statistical Mechanics* (Harper Collins Publishers, New York, 1976).
 - [62] J. P. Hansen and I. R. McDonald, *Theory of Simple Liquids* (Academic Press, London, 1986).
 - [63] L. Blum, *Mol. Phys.* **30**, 1529 (1975).
 - [64] L. Blum and J. S. Høye, *J. Phys. Chem.* **81**, 1311 (1977).
 - [65] K. Hiroike, *Mol. Phys.* **33**, 1195 (1977).
 - [66] L. Degève, M. Lozada-Cassou, E. Sánchez, and E. González-Tovar, *J. Chem. Phys.* **98**, 8905 (1993).
 - [67] L. Degève and M. Lozada-Cassou, *Mol. Phys.* **86**, 759 (1995).
 - [68] R. J. Hunter, *Zeta Potential in Colloid Science* (Academic Press, New York, 1981).
 - [69] F. Fenell-Evans and H. Wennerström, *The Colloidal Do-*

main: Where Physics, Chemistry, Biology and Technology Meet (Wiley-VCH, New York, 1994).

- [70] M. P. Allen and D. J. Tildesley, *Computer Simulation of Liquids* (Oxford University Press, New York, 1989).
- [71] D. Frenkel and B. Smit, *Understanding Molecular Simulation* (Academic Press, London, 2002).
- [72] L. Gierst, L. Vandenberghe, E. Nicolas, and A. Fraboni, *J. Electrochem. Soc.* **113**, 1025 (1966).
- [73] Y. G. Bérubé and P. L. de Bruyn, *J. Colloid Interface Sci.* **28**, 92 (1968).
- [74] T. Terao and T. Nakayama, *Phys. Rev. E* **63**, 041401 (2001).
- [75] S. H. Behrens, D.I. Christl, R. Emmerzael, P. Schurtenberger, and M. Borkovec, *Langmuir* **16**, 2566 (2000).

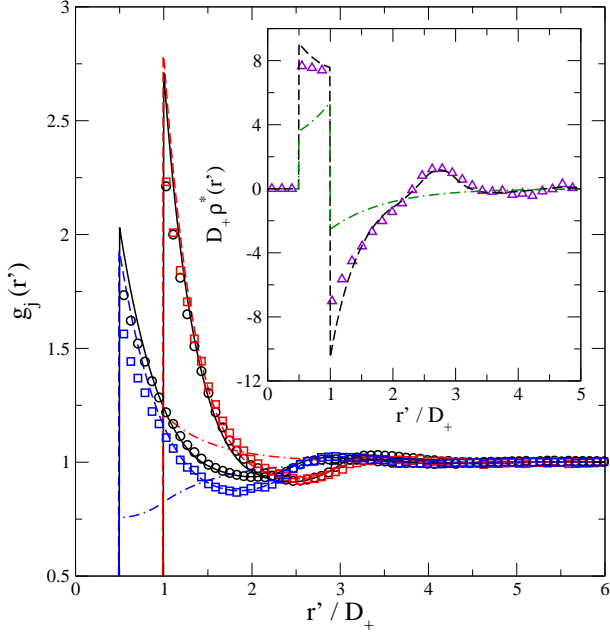


FIG. 1: Radial distribution functions of a size-asymmetric binary mixture of hard spheres and a size-asymmetric 1:1 electrolyte, both at a 1 M concentration, around an uncharged ($z_M = 0$) macroparticle (in the main panel). Thereinafter, the diameters of the ionic species and colloid are $D_+ = 4.25 \text{ \AA}$, $D_- = 8.5 \text{ \AA}$, and $D_M = 20 \text{ \AA}$, respectively. The small hard spheres have the same diameter as that of the cations, $D_1 = D_+$, and the large hard spheres diameter is the same as that of the anions, $D_2 = D_-$. The open circles correspond to Monte Carlo (MC) simulations of the size-asymmetric mixture of hard spheres and the open squares represent the MC data of the size-asymmetric monovalent electrolyte. The solid lines are associated to the asymmetric mixture of hard spheres in the HNC/MSA approach. The dashed and dot-dashed lines are the HNC/MSA and URMGC results for the 1:1 size-asymmetric salt, respectively. In the inset we depict the corresponding local electrolyte charge density for the 1:1 electrolyte case. Open triangles, and dashed and dot-dashed lines correspond to simulations, and the HNC/MSA and URMGC theories, respectively. Here and in the rest of the figures, the distance r' is measured from the colloidal surface.

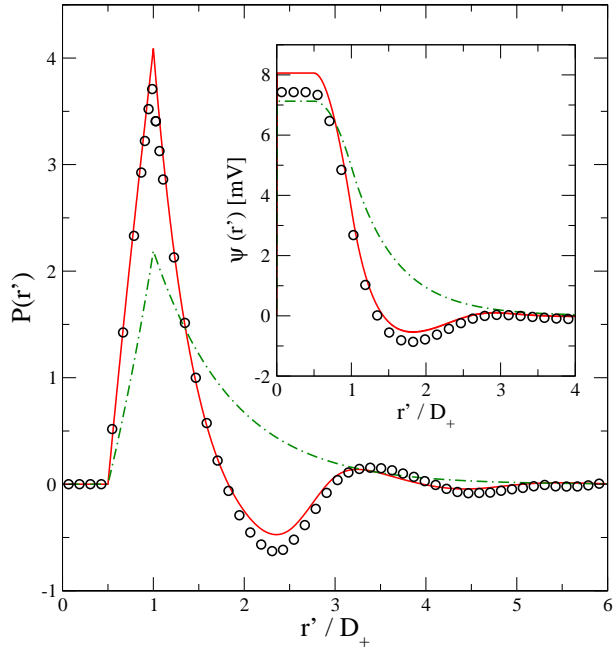


FIG. 2: Integrated charge (main panel) and mean electrostatic potential (inset) of a size-asymmetric 1:1, 1 M electrolyte around an uncharged ($z_M = 0$) macroparticle. The open circles, solid and dot-dashed lines correspond to the MC, HNC/MSA and URMGC data, respectively.

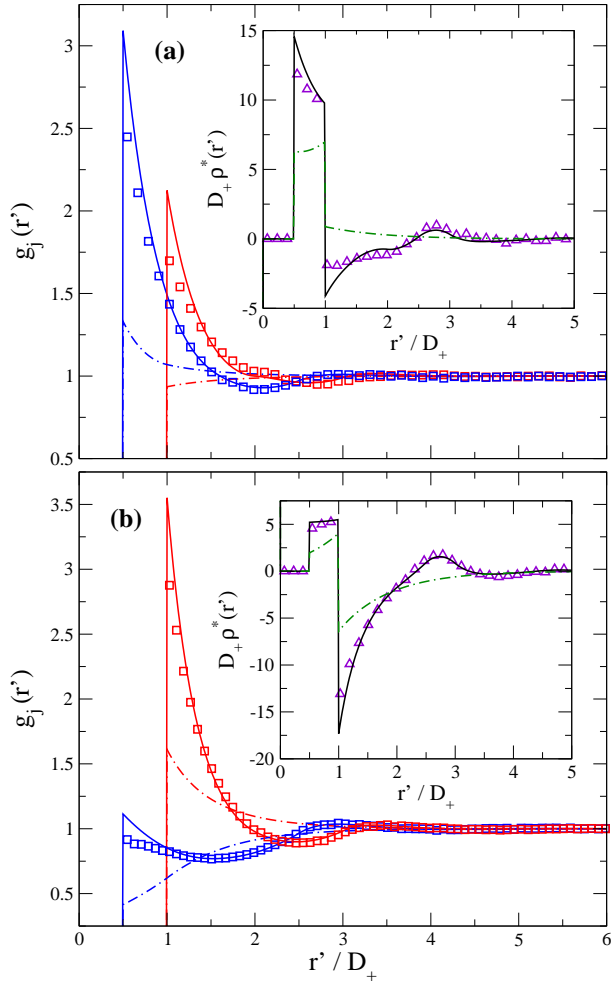


FIG. 3: Radial distribution functions of a size-asymmetric 1:1, 1 M electrolyte, around a charged macroion (main panel). In Fig. 3(a) $z_M = -4$, and in Fig. 3(b) $z_M = 4$. The open squares, solid and dot-dashed lines represent the MC, HNC/MSA and URMGC results, respectively. In the insets the corresponding local electrolyte charge densities are portrayed. Open triangles, and solid and dot-dashed lines are associated to simulations, and the HNC/MSA and URMGC theories, respectively.

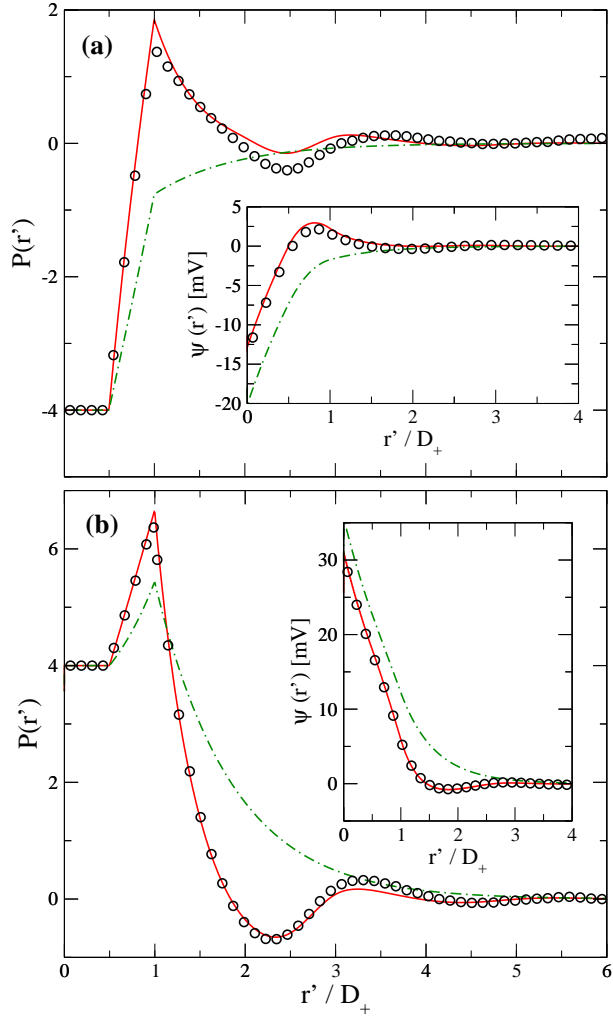


FIG. 4: Integrated charge (main panel) and mean electrostatic potential (inset) of a size-asymmetric 1:1, 1 M electrolyte around a charged macroion. In Fig. 4(a) $z_M = -4$, and in Fig. 4(b) $z_M = 4$. The open circles, solid and dot-dashed lines correspond to the MC, HNC/MSA and URMGC data, respectively.

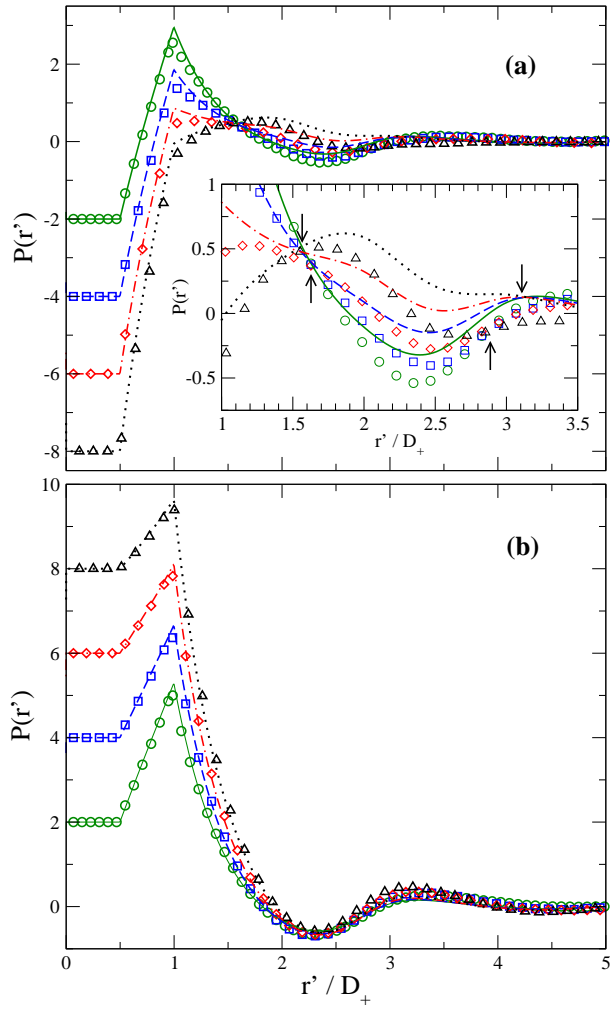


FIG. 5: Integrated charge of a size-asymmetric 1:1, 1 M electrolyte around a charged macroion. In Fig. 5(a) the open circles, squares, diamonds and triangles correspond to Monte Carlo simulations for $z_M = -2, -4, -6, -8$, respectively, and in Fig. 5(b) are associated to $z_M = 2, 4, 6, 8$, respectively. In Fig. 5(a) the solid, dashed, dot-dashed and dotted lines correspond to HNC/MSA results for $z_M = -2, -4, -6, -8$, respectively, and in Fig. 5(b) are associated to $z_M = 2, 4, 6, 8$, respectively.

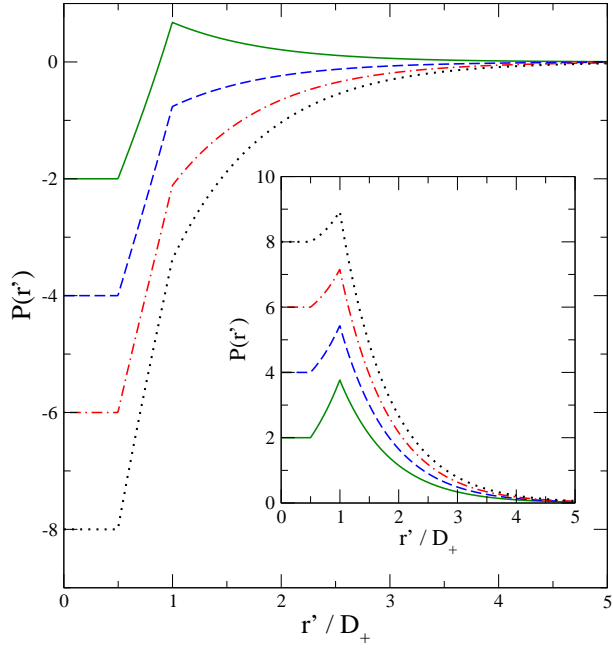


FIG. 6: The same as in Fig. 5 but for the URMGC theory. In the main figure the solid, dashed, dot-dashed and dotted lines correspond to $z_M = -2, -4, -6, -8$, respectively, and in the inset to $z_M = 2, 4, 6, 8$, respectively.

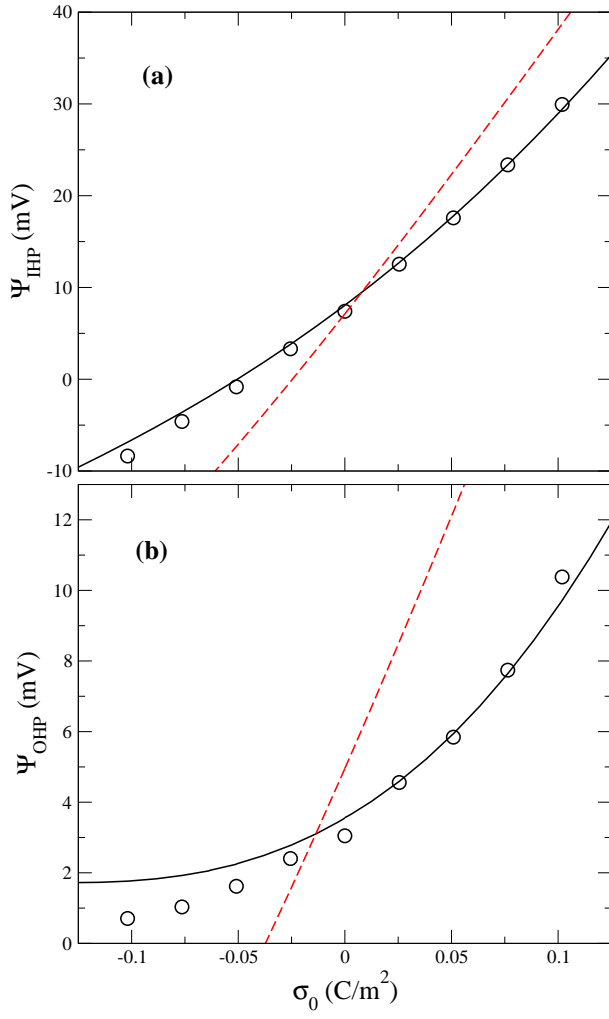


FIG. 7: Mean electrostatic potential (MEP) at the Helmholtz planes as functions of the surface charge density of a macroion immersed in a size-asymmetric 1:1, 1 M electrolyte. The open circles, and solid and dashed lines correspond to simulations, and the HNC/MSA and URMGC theories, respectively. In Fig. 7(a) the MEP at the IHP is plotted, and in the Fig. 7(b) the same is done for the MEP at the OHP.

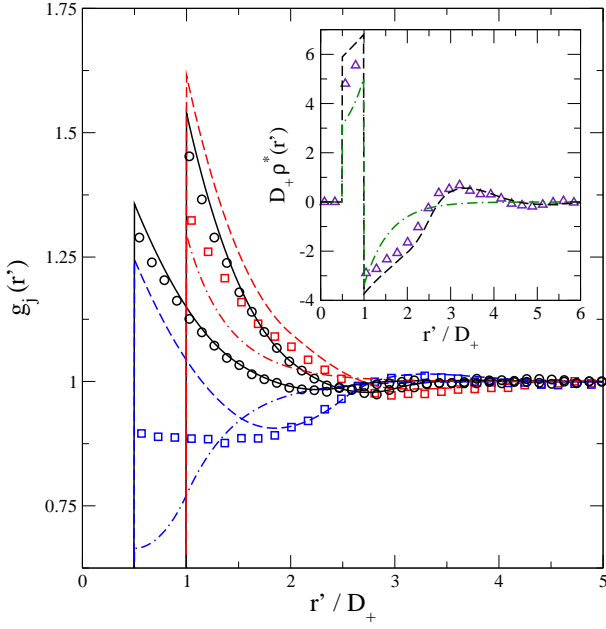


FIG. 8: Radial distribution functions of a size-asymmetric binary mixture of hard spheres and a size-asymmetric 2:2 electrolyte, both at a 0.5 M concentration, around an uncharged ($z_M = 0$) macroparticle (in the main panel). The small hard spheres have the same diameter as that of the cations, $D_1 = D_+$, and the large hard spheres diameter is the same as that of the anions, $D_2 = D_-$. The open circles correspond to Monte Carlo (MC) simulations of the size-asymmetric mixture of hard spheres and the open squares represent the MC data of the size-asymmetric divalent electrolyte. The solid lines are associated to the asymmetric mixture of hard spheres in the HNC/MSA approach. The dashed and dot-dashed lines are the HNC/MSA and URMGC results for the 2:2 size-asymmetric salt, respectively. In the inset we depict the corresponding local electrolyte charge density for the 2:2 electrolyte case. Open triangles, and dashed and dot-dashed lines correspond to simulations, and the HNC/MSA and URMGC theories, respectively.

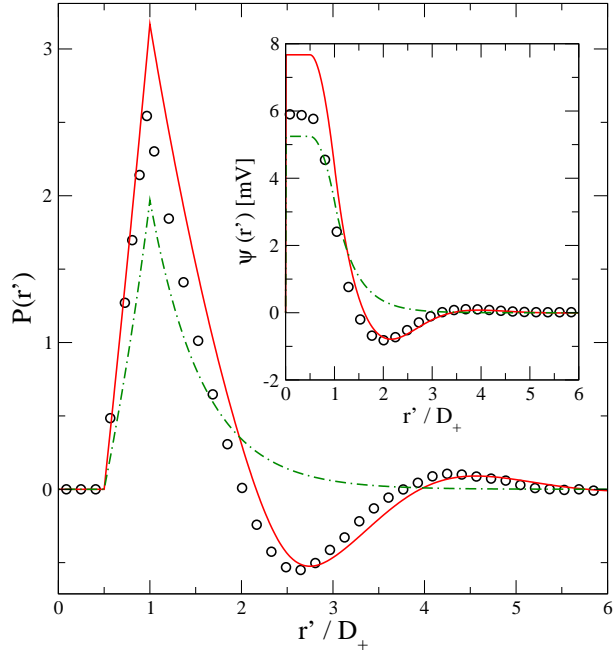


FIG. 9: Integrated charge (main panel) and mean electrostatic potential (inset) of a size-asymmetric 2:2, 0.5 M electrolyte around an uncharged ($z_M = 0$) macroparticle. The open circles, solid and dot-dashed lines are associated to the MC, HNC/MSA and URMGC data, respectively.

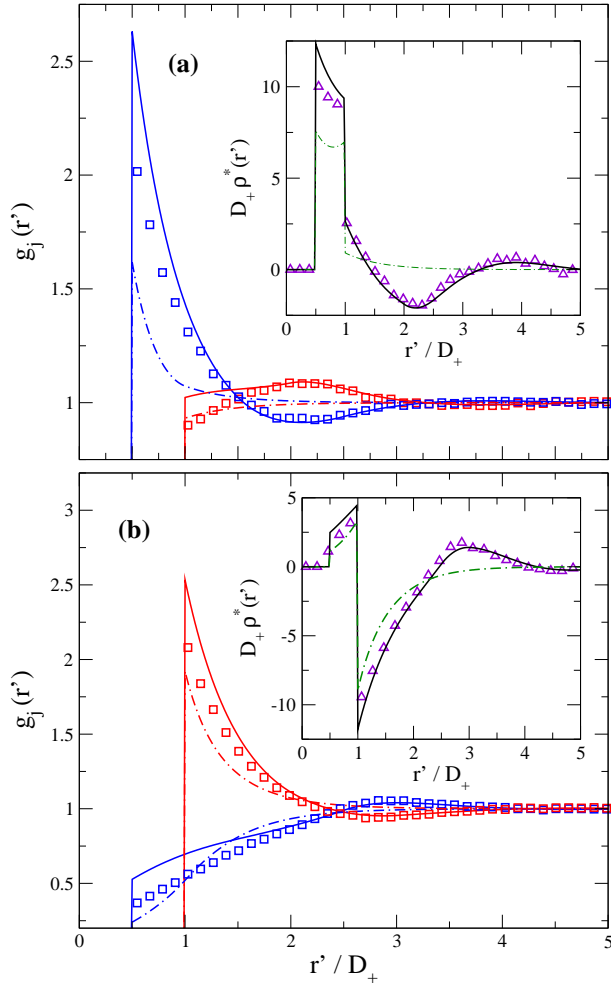


FIG. 10: Radial distribution functions of a size-asymmetric 2:2, 0.5 M electrolyte, around a charged macroion (main panel). In Fig. 10(a) $z_M = -4$, and in Fig. 10(b) $z_M = 4$. The open squares, solid and dot-dashed lines represent the MC, HNC/MSA and URMGC results, respectively. In the insets the corresponding local electrolyte charge densities are portrayed. Open triangles, and solid and dot-dashed lines are associated to simulations, and the HNC/MSA and URMGC theories, respectively.

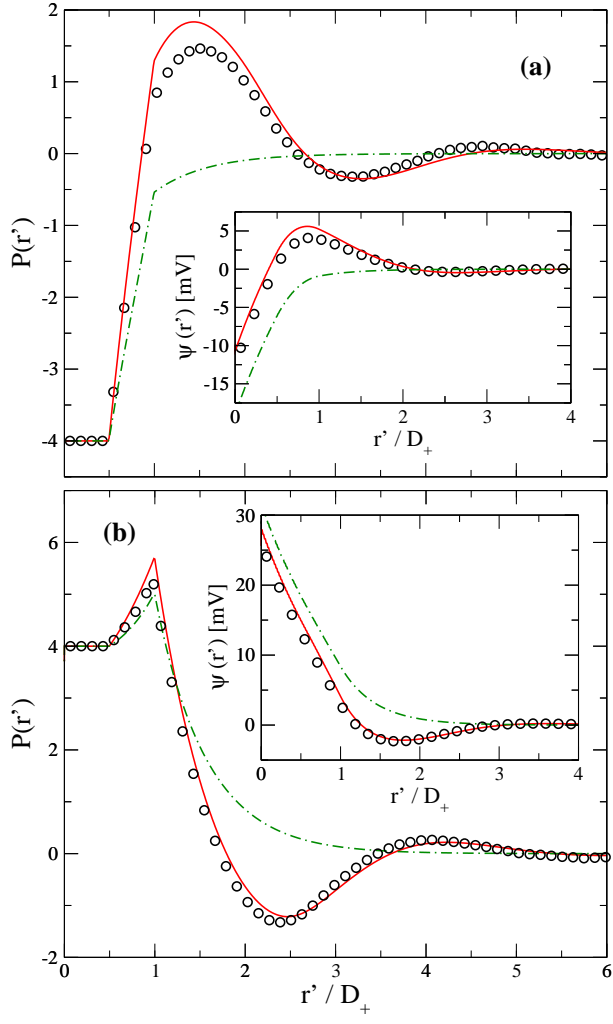


FIG. 11: Integrated charge (main panel) and mean electrostatic potential (inset) of a size-asymmetric 2:2, 0.5 M electrolyte around a charged macroion. In Fig. 11(a) $z_M = -4$, and in Fig. 11(b) $z_M = 4$. The open circles, solid and dot-dashed lines correspond to the MC, HNC/MSA and URMGC data, respectively.

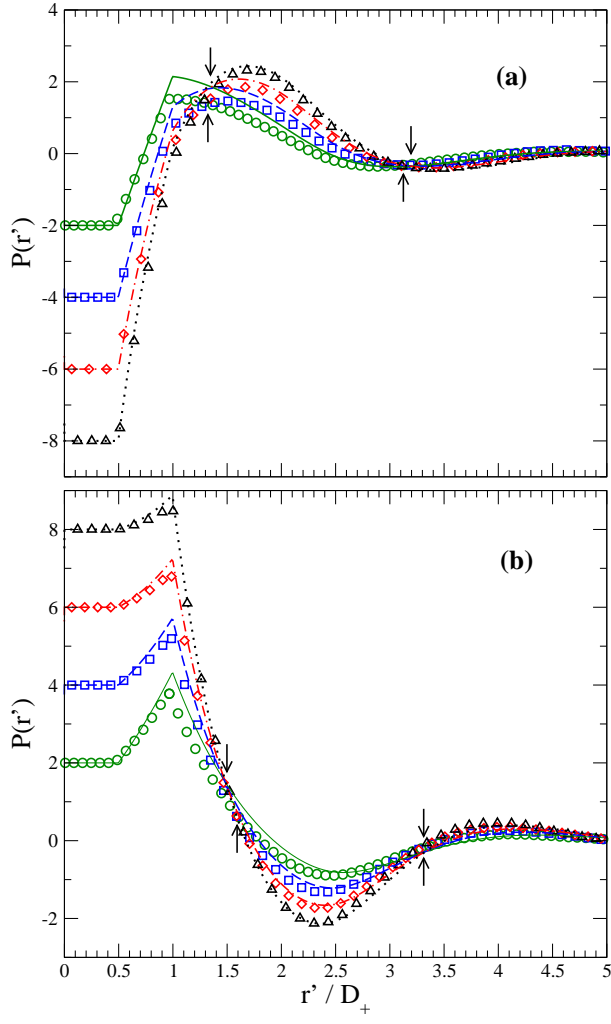


FIG. 12: Integrated charge of a size-asymmetric 2:2, 0.5 M electrolyte around a charged macroion. In Fig. 12(a) the open circles, squares, diamonds and triangles correspond to Monte Carlo simulations for $z_M = -2, -4, -6, -8$, respectively, and in Fig. 12(b) are associated to $z_M = 2, 4, 6, 8$, respectively. In Fig. 12(a) the solid, dashed, dot-dashed and dotted lines correspond to HNC/MSA results for $z_M = -2, -4, -6, -8$, respectively, and in Fig. 12(b) are associated to $z_M = 2, 4, 6, 8$, respectively.

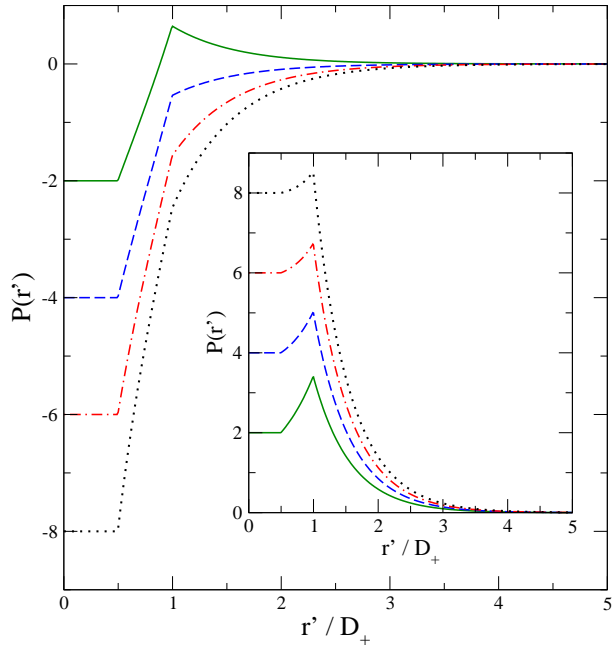


FIG. 13: The same as in Fig. 12 but for the URMGC theory. In the main figure the solid, dashed, dot-dashed and dotted lines correspond to $z_M = -2, -4, -6, -8$, respectively, and in the inset to $z_M = 2, 4, 6, 8$, respectively.

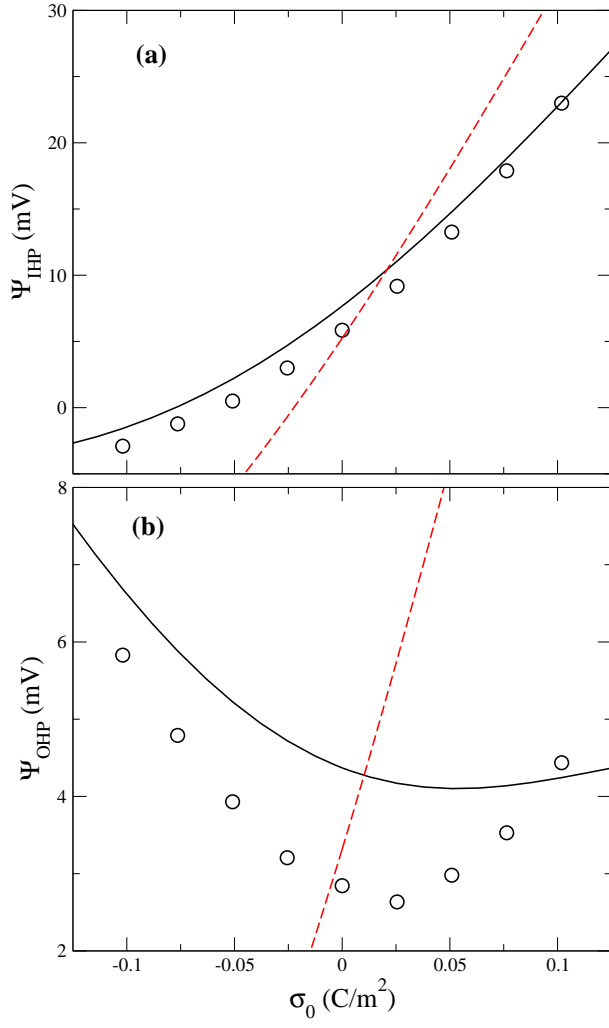


FIG. 14: Mean electrostatic potential (MEP) at the Helmholtz planes as functions of the surface charge density of a macroion immersed in a size-asymmetric 2:2, 0.5 M electrolyte. The open circles, and solid and dashed lines correspond to simulations, and the HNC/MSA and URMGC theories, respectively. In Fig. 14(a) the MEP at the IHP is plotted, and in the Fig. 14(b) the same is done for the MEP at the OHP.

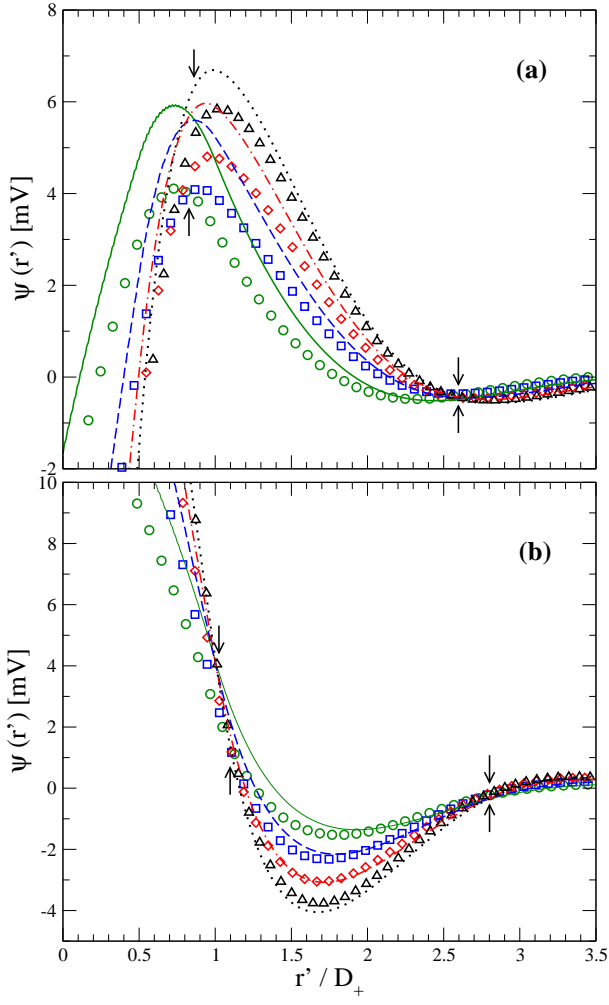


FIG. 15: Mean electrostatic potential of a size-asymmetric 2:2, 0.5 M electrolyte around a charged macroion. In Fig. 15(a) the open circles, squares, diamonds and triangles correspond to Monte Carlo simulations for $z_M = -2, -4, -6, -8$, respectively, and in Fig. 15(b) are associated to $z_M = 2, 4, 6, 8$, respectively. In Fig. 15(a) the solid, dashed, dot-dashed and dotted lines correspond to HNC/MSA results for $z_M = -2, -4, -6, -8$, respectively, and in Fig. 15(b) are associated to $z_M = 2, 4, 6, 8$, respectively.